Tectonophysics 647–648 (2015) 112–131

Contents lists available at ScienceDirect

Tectonophysics

journal homepage: www.elsevier.com/locate/tecto

Quality assessment of reservoirs by means of outcrop data and "discrete fracture network" models: The case history of *Rosario de La Frontera* (NW Argentina) geothermal system

R. Maffucci[a,*], S. Bigi[b], S. Corrado[a], A. Chiodi[c], L. Di Paolo[d], G. Giordano[a,e], C. Invernizzi[f]

[a] *Dipartimento di Scienze, Università Roma Tre, 00146 Roma, Italy*
[b] *Department of Earth Sciences, Sapienza University of Rome, Italy*
[c] *GEONORTE-INENCO (UNSa-CONICET), Av. Bolivia 5150, A4400FVY Salta, Argentina*
[d] *Geology and Geochemistry Labs (GEOLAB), ENI E&P Division, 20097 San Donato Milanese, MI, Italy*
[e] *Istituto per la Dinamica dei Processi Ambientali, Sezione di Milano, Consiglio Nazionale delle Ricerche, Milano, Italy*
[f] *Scuola di Scienze e Tecnologie, Sezione di Geologia, Università degli studi di Camerino, 62032 Camerino, MC, Italy*

ARTICLE INFO

Article history:
Received 12 May 2014
Received in revised form 13 February 2015
Accepted 16 February 2015
Available online 28 February 2015

Keywords:
Reservoir
DFN modeling
Geothermal system
Faults and fractures
Rosario de La Frontera
NW Argentina

ABSTRACT

We report the results of a systematic study carried out on the fracture systems exposed in the *Sierra de La Candelaria* anticline, in the central Andean retrowedge of northwestern Argentina. The aim was to elaborate a kinematic model of the anticline and to assess the dimensional and spatial properties of the fracture network characterizing the Cretaceous sandstone reservoir of the geothermal system of *Rosario de La Frontera*. Special regard was devoted to explore how tectonics may affect fluid circulation at depth and control fluids' natural upwelling at surface. With this aim we performed a Discrete Fracture Network model in order to evaluate the potential of the reservoir of the studied geothermal system. The results show that the *Sierra de La Candelaria* regional anticline developed according to a kinematic model of transpressional inversion compatible with the latest Andean regional WNW–ESE shortening, acting on a pre-orogenic N–S normal fault. A push-up geometry developed during positive inversion controlling the development of two minor anticlines: *Termas* and *Balboa*, separated by further NNW–SSE oblique-slip fault in the northern sector of the regional anticline. Brittle deformation recorded at the outcrop scale is robustly consistent with the extensional and transpressional events recognized at regional scale. In terms of fluid circulation, the NNW–SSE and NE–SW fault planes, associated to the late stage of the positive inversion, are considered the main structures controlling the migration paths of hot fluids from the reservoir to the surface. The results of the fracture modeling performed show that fractures related to the same deformation stage, are characterized by the highest values of secondary permeability. Moreover, the DFN models performed in the reservoir volume indicates that fracture network enhances its permeability: its secondary permeability is of about 49 mD and its fractured portion represents the 0.03% of the total volume.

1. Introduction

The characterization of naturally fractured reservoirs continues to challenge geoscientists due to their complexity and unpredictable nature (Nelson, 1998; Jafari and Babadagli, 2011). Furthermore, naturally occurring fractures have significant effects on reservoir fluid flow (Evans and Hobbs, 2003; Roure et al., 2005, 2010; Fischer et al., 2009; Bjørlykke, 2010; Faulkner et al., 2010; Beaudoin et al., 2011; Barbier et al., 2012; Evans and Fischer, 2012; Bigi et al., 2013). As a matter of fact not only they could increase or decrease the permeability of many reservoirs worldwide, but also may induce significant permeability anisotropy due to their geometry and type (Aydin, 2000). For this reason, a correct evaluation of reservoirs means to obtain the best understanding of its fracture network in order to analyze the effects on fluid flow (Guerriero et al., 2010, 2011, 2013, and references therein). As a consequence, this is also a key target for the exploitation of water dominated geothermal reserves (Grant et al., 1982; Brogi et al., 2003; Vignaroli et al., 2013; Giordano et al., 2014).

The classification of naturally fractured reservoirs based on the relationship between primary and secondary porosity and permeability proposed by Nelson (1992) is generally accepted. Particular attention must be paid in the evaluation of those reservoirs where fractures produce significant reservoir anisotropy (barriers) creating compartmentalization instead of providing additional porosity and/or permeability (Odling et al., 1999; Aydin, 2000; Jolley et al., 2010; Manzocchi et al., 2010). Having granular material the potential to develop particularly low porosity deformation zones (Antonellini and Aydin, 1994; Aydin, 2000), their occurrence in sandstone reservoir can reduce permeability of some orders of magnitude when compared

* Corresponding author. Tel.: +39 0657338082.
E-mail address: roberta.maffucci@uniroma3.it (R. Maffucci).

http://dx.doi.org/10.1016/j.tecto.2015.02.016
0040-1951/

to that of the undeformed hosting rock (Matthai et al., 1998; Fossen and Bale, 2007; Sternlof et al., 2004). Therefore, an accurate classification of fractures and a quantitative evaluation of the fracture network have a direct impact on the development planning of geothermal fields, because production may strongly depend on the permeability anisotropy created by fractures.

Discrete Fracture Network (DFN) modeling (Dershowitz and Einstein, 1988; Cacas et al., 1990; Watanabe and Takahashi, 1995) represents an important tool during exploration and exploitation phases of fractured reservoirs. It is widely accepted that it provides an accurate prediction of the fracture network since it accepts as input data, statistical and probabilistic information on fracture properties, obtained by means of systematic fracture field mapping.

In this framework, the reliability of fracture system characterization highly depends on the quality of mapping and of outcrop conditions, especially in the case of limited extension of rock exposures and/or limited depths of boreholes. For this reason, a variety of methodologies for both data acquisition and analysis have been developed, from outcrop/well scale to regional/seismic scale, in order to provide the best criteria for predicting fracture networks (Van Dijk, 1998). Some acquisition techniques are based on the characterization of outcropping structures as analogues for subsurface portions of the reservoirs (Hennings et al., 2000; Belayneh et al., 2006; Laubach and Ward, 2006; Barr et al., 2007). These techniques comprise the acquisition of fracture data along scan-lines (e.g. Priest and Hudson, 1981; Zeeb et al., 2013; Bisdom et al., 2014 among many others), and on scan-areas (e.g. Pahl, 1981; Marchegiani et al., 2006), at outcrop scale, in order to elaborate a probabilistic model representing fracture distribution at reservoir scale and some tools that are more modern such as the light detection and ranging technique (LiDAR, or laserscan) and new, effective developments in phogrammetry (Tavani et al., 2014).

In this work, we have applied scan-line acquisition technique in order to collect structural data to assess the quality of the geothermal reservoir of *Rosario de La Frontera* system, belonging to the *Sierra de La Candelaria* anticline, one of the positively inverted structures cropping out between the provinces of Salta and Tucuman (NW Argentina). The purpose of this approach is to compute its secondary permeability in order to predict the reservoir behavior in prospect evaluation and reservoir management.

The Cretaceous deposits of the *Salta* Group (*Pirgua* Subgroup), provide the reservoir of this active geothermal system (Moreno Espelta et al., 1975; Seggiaro et al., 1995; Seggiaro et al., 1997; Maffucci et al., 2012b, 2013; Invernizzi et al., 2014). It consists of continental deposits, mainly represented by sandstones and conglomerates, related to the syn-rift stage (Late Neocomian–Early Maastrichtian) (Salfity and Marquillas, 1994; Marquillas et al., 2005). In the area, they are deformed in a N–S trending hangingwall anticline (*Sierra de La Candelaria*) and dissected by subsequently strike-slip and normal faults.

The anticline and the associated deformative structures (faults and fractures) represent the structural backbone of the studied geothermal system.

2. Geological setting

Sierra de La Candelaria ridge is located in the foothills of the Central Andean retro-wedge, in the Salta province (NW Argentina) between the Eastern Cordillera to the west and the southern segment of the Santa Bárbara System to the east (Fig. 1).

These units are characterized by a basement-involved thrust system (Baldis et al., 1976; Rolleri, 1976; Allmendiger et al., 1983; Jordan et al., 1983; Cahill et al., 1992; Kley and Monaldi, 1998; Seggiaro and Hongn, 1999), resulting from an eastward migrating shortening that occurred during Miocene–Quaternary times (Grier et al., 1991; Salfity et al., 1993; Kress, 1995; Cristallini et al., 1997; Kely and Monaldi, 2002; Allmendiger and Gubbels, 1996; Kley and Monaldi, 1999; Reynolds et al., 2000; Kley and Monaldi, 2002).

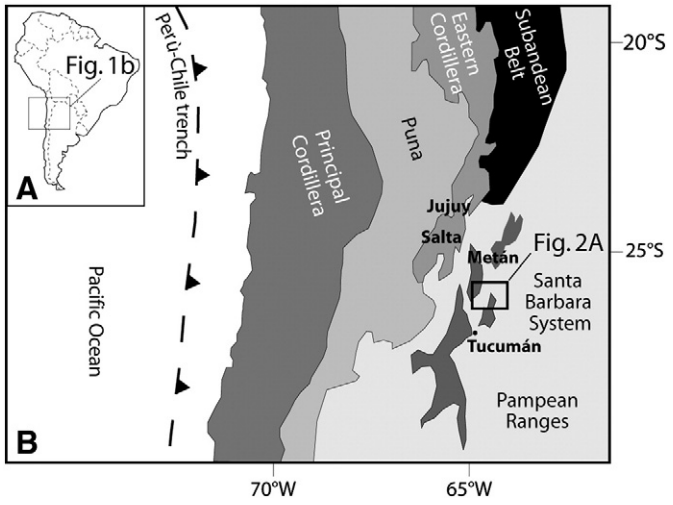

Fig. 1. Map illustrating the geological provinces of northwest Argentina, modified from Carrera and Muñoz (2008).

As a result, the Andean structure in this area is dominated by broad, low-amplitude folds, generated in the hangingwall of east-verging high-angle thrust faults (Kley and Monaldi, 2002; Mon and Gutierréz, 2007; Norini et al., 2013) mainly due to the Andean inversion of pre-existing normal faults generated during the Cretaceous rifting event (Bianucci et al., 1982; Grier et al., 1991; Carrera et al., 2006).

Sierra de La Candelaria ridge represents one of these broad anticlines that is elongated in N–S direction for about 55 km and with a maximum elevation of about 2600 m a.s.l. (Fig. 2A; González et al., 2000; Salfity and Monaldi, 2006). The main structural feature responsible of its uplift is a high-angle reverse fault plane dipping to the west with top-to-the-east sense of transport that borders the anticline along its eastern margin (Moreno Espelta et al., 1975; Seggiaro et al., 1997). It is interpreted as an inverted normal fault inherited from the rifting stage (Iaffa et al., 2013).

The stratigraphy of the geothermal system covers a wide time span: from pre-Cambrian to Pliocene–Quaternary times (Fig. 2B). The older stratigraphic unit crops out in the core of the anticline. It is the Precambrian basement made up of low grade metasedimentary rocks (*Medina* Formation) that, in the northern portion and along the western limb of the anticline, is unconformably overlain by a thick succession of continental Cretaceous to Paleogene strata (*Salta* Group) related to the Cretaceous rift stage (Turner, 1959; Salfity, 1982; Galliski and Viramonte, 1988; Salfity and Marquillas, 1994; Viramonte et al., 1999; Marquillas et al., 2005). The Early to Late Cretaceous *Pirgua* subgroup, marks the syn-rift fill stage (Salfity and Marquillas, 1994), whereas the *Balbuena* and *Santa Bárbara* subgroups represent the post-rift thermal subsidence stage (Bianucci et al., 1981; Salfity and Marquillas, 1994; Comníguez and Ramos, 1995). Post-rift deposits are in turn overlain by a thick continental foreland basin fill, related to the Andean mountain uplift and erosion, that was deposited from Middle Miocene to Pliocene–Quaternary times (Gebhard et al., 1974). The retrowedge basin fill includes two subgroups (*Metán* and *Jujuy*, according to Gebhard et al., 1974) belonging to the *Orán* Group. The main outcrops of these subgroups cover the northern portion of *Sierra de La Candelaria* ridge at the lowest elevations.

The stratigraphic succession cropping out along the *Sierra de La Candelaria* ridge forms an anticline whose general trend is N–S (Fig. 2A). In detail, this trend is characterized by a NNE to NNW change of the longitudinal axis moving from south to north as a result of the two regional E–W and WNW–ESE shortening directions occurred during the Andean compression (Marrett et al., 1994; Iaffa et al., 2011). In addition, the northern portion of the anticline is offset by several minor faults. The most important is a NNW–SSE trending high angle fault that divides the structure in two anticlines: *Termas* and *Balboa* (Moreno Espelta et al.,

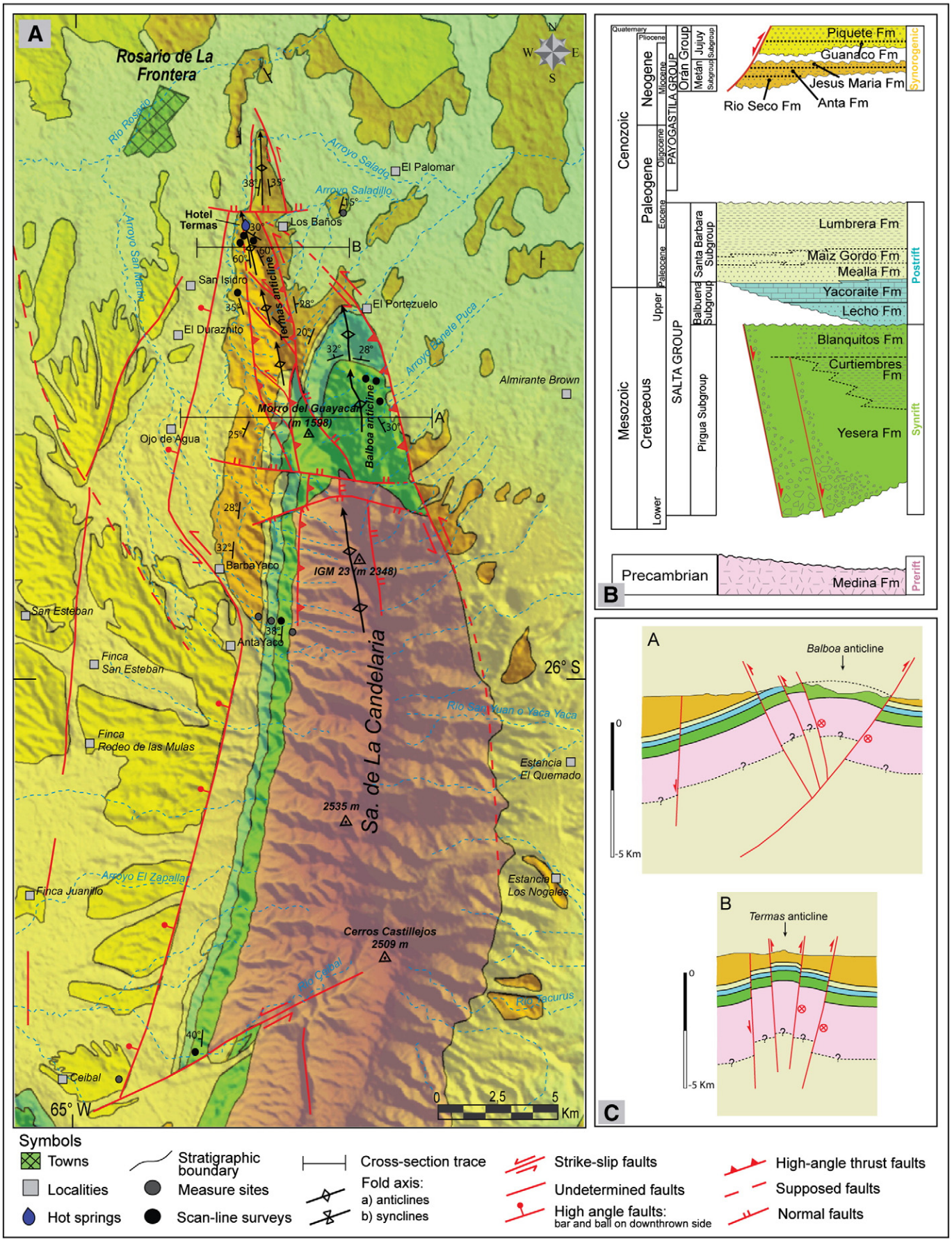
A
Rosario de La Frontera
Río Rosario
Arroyo Salado
El Palomar
Arroyo Saladillo
Hotel Termas
Los Baños
Arroyo San Ignacio
San Isidro
Termas anticline
El Portezuelo
El Durazno
Arroyo Banete Puca
Almirante Brown
Morro del Guayacán (m 1598)
Balboa anticline
Ojo de Agua
BarbaYaco
IGM 23 (m 2348)
San Esteban
Anta Yaco
Finca San Esteban
26° S
Río San Juan o Yaca Yaca
Finca Rodeo de las Mulas
Estancia El Quemado
2535 m
Sa. de La Candelaria
Arroyo El Zapallar
Finca Juanillo
Estancia Los Nogales
Cerros Castillejos 2509 m
Río Caibal
Río Yacurus
Ceibal
65° W
0 2.5 5 Km
B
Cenozoic
Mesozoic
Quaternary
Pliocene
Neogene
Miocene
Oligocene
Paleogene
Eocene
Paleocene
Upper
Cretaceous
Lower
PAYOGASTILA GROUP
Orán Group
Metán Subgroup
Jujuy Subgroup
SALTA GROUP
Santa Barbara Subgroup
Balbuena Subgroup
Pirgua Subgroup
Piquete Fm
Guanaco Fm
Jesus Maria Fm
Anta Fm
Río Seco Fm
Synorogenic
Lumbrera Fm
Maíz Gordo Fm
Mealla Fm
Yacoraite Fm
Lecho Fm
Postrift
Blanquitos Fm
Curtiembres Fm
Yesera Fm
Synrift
Precambrian
Medina Fm
Prerift
C
A
Balboa anticline
0
-5 Km
B
Termas anticline
0
-5 Km
Symbols
Towns
Localities
Hot springs
Stratigraphic boundary
Measure sites
Scan-line surveys
Cross-section trace
Fold axis:
a) anticlines
b) synclines
Strike-slip faults
Undetermined faults
High angle faults:
bar and ball on downthrown side
High-angle thrust faults
Supposed faults
Normal faults

1975; Seggiaro et al., 1997; Barcelona et al., 2014). The *Balboa* anticline, to the east, trends N–S and is characterized by the outcrops of Cretaceous sandstones of the *Pirgua* subgroup at its core (Figs. 2A, C, section A). Whereas the *Termas* anticline, to the west, trends NNW–SSE. At its core, where *Anta* Formation crops out, are located the hot springs, close to the thermal complex of the *Hotel Termas* (Figs. 2A, C, section B). They are characterized by surface temperatures ranging between 24.1 °C and 90.5 °C (Seggiaro et al., 1995; Pesce and Miranda, 2003; Chiodi et al., 2012a, b; Invernizzi et al., 2014). This northern segment is bordered to the south by an E–W inverted high-angle fault dipping to the north.

Further to the south, along the western fold limb of the regional anticline, a kilometric NE–SW strike-slip fault cross cuts the regional anticline and is marked by the *Ceibal* hot spring with temperature of about 38 °C.

Fractured sandstones belonging to the Cretaceous syn-rift deposits of the *Salta* Group provide the geothermal reservoir both in this area (Moreno Espelta et al., 1975; Seggiaro et al., 1995; Seggiaro et al., 1997; Maffucci et al., 2012b, 2013; Invernizzi et al., 2014) and in the region (Giordano et al., 2013). On the contrary, the low permeable post-rift and the syn-orogenic deposits (respectively, *Balbuena* and *Santa Bárbara* subgroup and *Metán* subgroup) are considered to act as cap rocks (Moreno Espelta et al., 1975; Seggiaro et al., 1995, 1997; Di Paolo et al., 2012; Maffucci et al., 2012b; Invernizzi et al., 2014).

3. Method

The method followed for the assessment of the studied geothermal reservoir consists of different steps mainly focused on the structural analysis at the outcrop scale and on fracture modeling (Fig. 3).

Field work was dedicated both to qualitative and quantitative analyses (orientation, dimension, spatial distributions, mode of deformation and spacing) of structural data recorded in the outcropping sedimentary succession. Structural data on faults, cleavages, fractures, and veins were collected at 95 georeferenced field sites in the *Sierra de La Candelaria* anticline (Fig. 2A). Measure sites were distributed in different areas of the anticline, along the forelimb, the backlimb and in the northern plunging nose, in order to illustrate the relationship of the structural data features to folding and their influence on fluid flow.

The first phase of our investigation consisted of geometric analysis of structures at the outcrop scale. Fractures were classified as longitudinal, transverse and oblique with respect to the fold axis trend (e.g. Cooper, 1992; Stearns, 1968; Hancock, 1985; Hennings et al., 2000) and so divided into different sets on the base of their orientation in order to perform the fracture modeling within the reservoir volume. Furthermore, a frequency distribution of fracture data within the anticline was obtained by the acquisition of spacing data derived from scan-line surveys (Priest and Hudson, 1981; Rouleau and Gale, 1985; Priest, 1993; Wu and Pollard, 1995). The method consists of counting the number of fractures per unit length along a sampling line. Spacing values of fracture sets were computed by applying the Terzaghi trigonometric correction, in order to reduce the measurement bias (Terzaghi, 1964). For each scan-line we also measured the attitude (dip-azimuth, dip angle), deformation mode and length of the different fractures in order to provide the main fracture system parameters subsequently used for the fracture modeling. In addition, owing to the long time required for the acquisition of scan-lines, in several localities fast scan-lines were also performed. They were carried out perpendicularly to each fracture set measuring only the spacing value of fractures. Features of the 15 scan lines and 5 fast scan lines performed are reported in Table 1.

The next step concerned the construction of a 3-D reservoir geological model representing the tectonic structure. The original data directly gathered during our fieldwork, together with the already published geological maps and schemes (Moreno Espelta et al., 1975; Seggiaro et al., 1997; González et al., 2000; Bercheñi, 2003; Salfity and Monaldi, 2006; Maffucci et al., 2013), were integrated to draw detailed geological cross sections across the *Sierra de La Candelaria* anticline, oriented normal and parallel to the fold axes trend (Fig. 4). The 3D reconstruction of the main geological surfaces (top and bottom of target reservoir, faults and thrust planes) allowed the built of the reservoir volume, subsequently converted into a geocellular volume. This latter consists of regular, defined size, grid-like cells that can be converted into equivalent properties (such as porosity and permeability) on the base of the fracture modeling performed through the upscaling process.

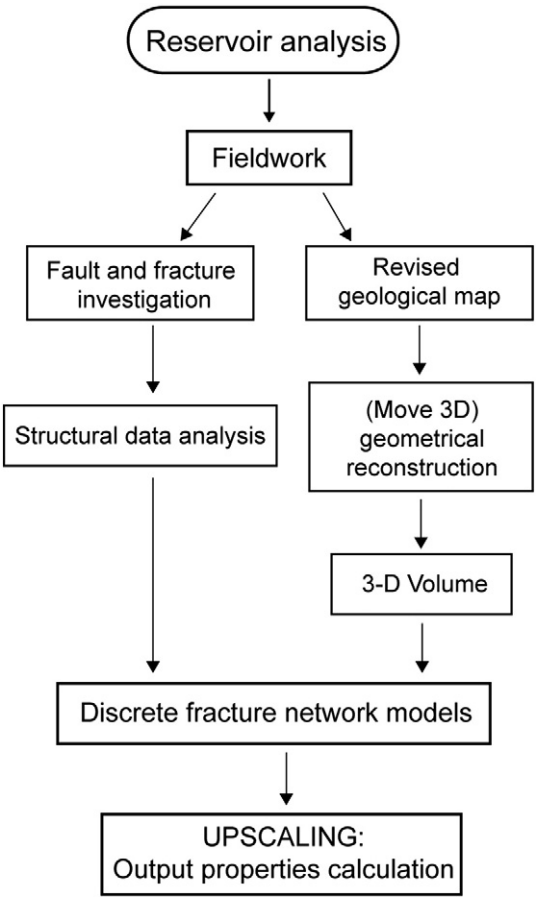

Fig. 3. Flow diagram illustrating the sequential steps followed in this study. Fieldwork and the 3-D software modeling are at the base of the work (see text for detailed explanation).

The fracture modeling process was based on the elaboration of field data in order to generate the DFN model in the 3-D volume of the geothermal reservoir.

4. Results

4.1. 3-D reservoir model

The accurate reconstruction of the *Sierra de La Candelaria* structure allows us to highlight the asymmetric shape of the anticline and to reconstruct in a 3-D view the structural framework of the geothermal fluid of *Rosario de La Frontera* system (Fig. 5).

In detail, the anticline is characterized by a gently dipping forelimb (30°) and a steeply westward dipping backlimb (60°). Its general

Fig. 2. (A) Geological Map of *Sierra de La Candelaria* anticline. (B) Chronostratigraphic column showing the tectonostratigraphic units cropping out in the study area, as well as the main tectonic events that controlled their deposition (redrawn by Carrera et al., 2006). (C) Representative cross sections of the anticline. Their location is indicated in the geological map.

Table 1
Summary of data for scan lines (SL) and fast scan lines (FSL) carried out on the outcropping reservoir (R) and cap rocks (C) of the geothermal system.

Survey type	Longitude	Latitude	Rock type	Dip direction/dip angle	Length (cm)	Number of data
SL 1	−25.83554	−64.93138	CR	255/15	1000	81
SL 2	−25.83833	−64.93341	CR	330/05	1000	40
SL 3	−25.83650	−64.93487	CR	10/0	750	78
SL 4	−25.83790	−64.93052	CR	30/10	527	17
SL 5	−25.83461	−64.93719	CR	20/0	903	49
SL 6	−25.83854	−64.93333	CR	220/10	500	39
SL 7	−25.99150	−64.91741	R	290/15	490	15
SL 8	−25.98974	−64.91750	R	110/05	600	20
SL 9	−25.99024	−64.91951	R	280/05	1000	30
SL 10	−25.98809	−64.91719	R	340/25	990	21
SL 11	−25.97931	−64.93237	CR	100/10	976	91
SL 12	−25.83884	−64.93100	CR	30/0	452	26
SL 13	−25.89127	−64.87830	R	280/03	770	20
SL 14	−25.88923	−64.87990	R	310/03	940	35
SL 15	−26.14929	−64.95553	R	150/0	660	40
FSL 1	−25.83790	−64.93389	CR	310/60	200	9
FSL 2	−25.98981	−64.92008	R	170/0	200	14
FSL 3	−25.98804	−64.91776	R	210/50	97	10
FSL 4	−25.88990	−64.88186	R	74/0	96	16
FSL 5	−25.90636	−64.87943	R	100/0	63	11

trend is N–S but further to the north it turns to a NNW–SSE orientation in the axial plunging of the *Hotel Termas* area.

The eastern limb of the anticline is bounded by the high-angle reverse fault striking N–S with a top-to-the-east sense of transport (Fig. 5A). This fault plane and a backthrust on the western limb, striking N–S and dipping to the east, are the main faults responsible of the uplift of the anticline.

Furthermore, the anticline is offset by several minor faults. To the north, the anticline core is truncated by a NNW–SSE trending oblique-slip fault with a left-lateral strike-slip component; in the western area, the backlimb is affected by a series of minor NW–SE trending faults characterized by left-lateral strike-slip transtensional kinematic. In the southern reconstructed sector along the western limb, a kilometric NE–SW left-lateral strike-slip fault borders the reservoir and is marked by the *Ceibal* hot spring.

In a 3-D reconstruction we propose a possible confinement of the reservoir continuity at depth, in particular on the western side of the main anticline, calculating a minimum conservative volume of the reservoir's deposits (Figs. 5B, C). It is delimited to the east by the main high angle thrust fault that borders the anticline on the eastern side. To the north, it is confined by the normal fault plane trending E–W and dipping to the north (Barcelona et al., 2013, 2014), and to the west by a continuous, almost N–S oriented, lineament well visible on remote sensing images (Invernizzi et al., 2014). To the south, the reservoir is confined by the outcrops of *Pirgua* subgroup and by the NE–SW strike-slip fault occurring in the *Ceibal* area. Therefore, it can be assumed that the Cretaceous sandstones, that form the main geothermal reservoir, consist of a single and continuous hydrogeothermal body with an estimated volume of about 53 km^3 and a mean thickness of about 450 m (Fig. 5D). The maximum depths reached by the top and bottom surfaces of *Pirgua* subgroup are 2000 m and 2450 m, respectively (Figs. 5B, C). They are calculated in the northern sector of the anticline, along its western margin.

4.2. Structural data at the outcrop scale

The field surveys were performed in different structural domains along the *Sierra de La Candelaria* ridge: backlimb, forelimb and plunging northern nose of the two northern anticlines. In detail, structural data were collected in the *Guanaco*, *Jesús María*, *Anta*, *Yacoraite*, *Pirgua* and *Medina* Formations. The first three formations are mainly exposed in the northern portion of the ridge; *Anta* Formation extensively crops out both in the crestal sector of *Termas* anticline and along the western limb of the main anticline. On the contrary, *Yacoraite* Formation and *Pirgua* Subgroup are widely exposed along the limbs in the central sector of *Balboa* anticline and in the southern sector of the ridge.

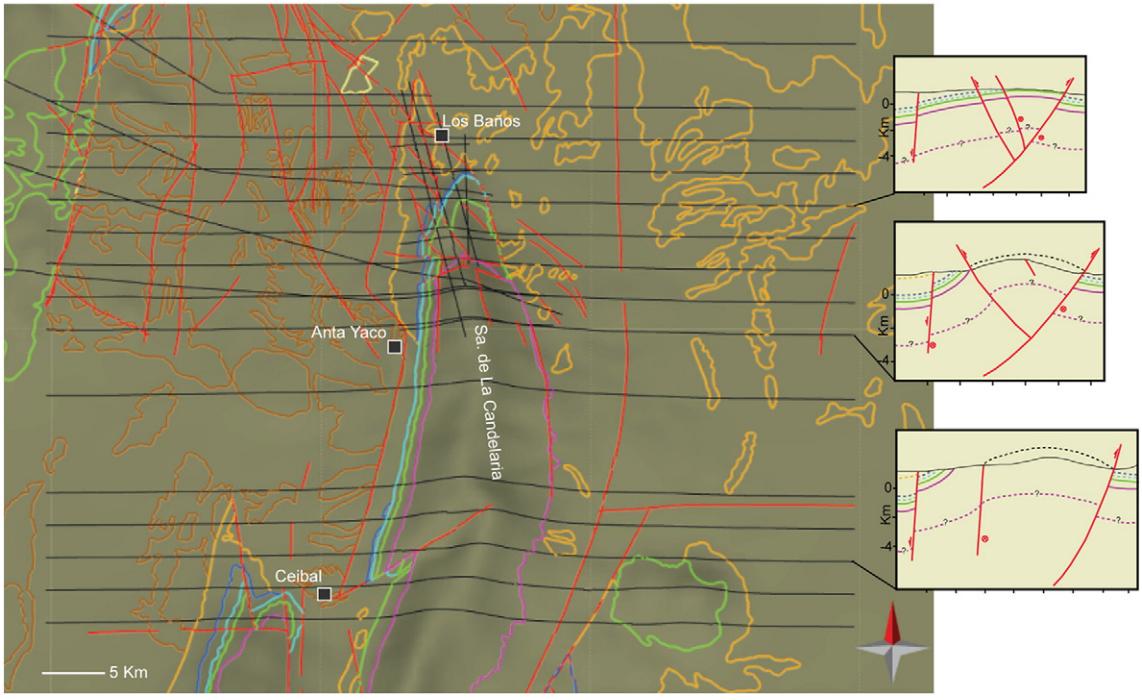

Fig. 4. Traces of the geological cross sections (black lines) and map used to construct the three-dimensional structural model. In the gray panels are some examples of geological cross sections. Continuous pink and green lines represent top and bottom of the *Medina* Formation and *Pirgua* Subgroup, respectively. They were used to build the reservoir volume.

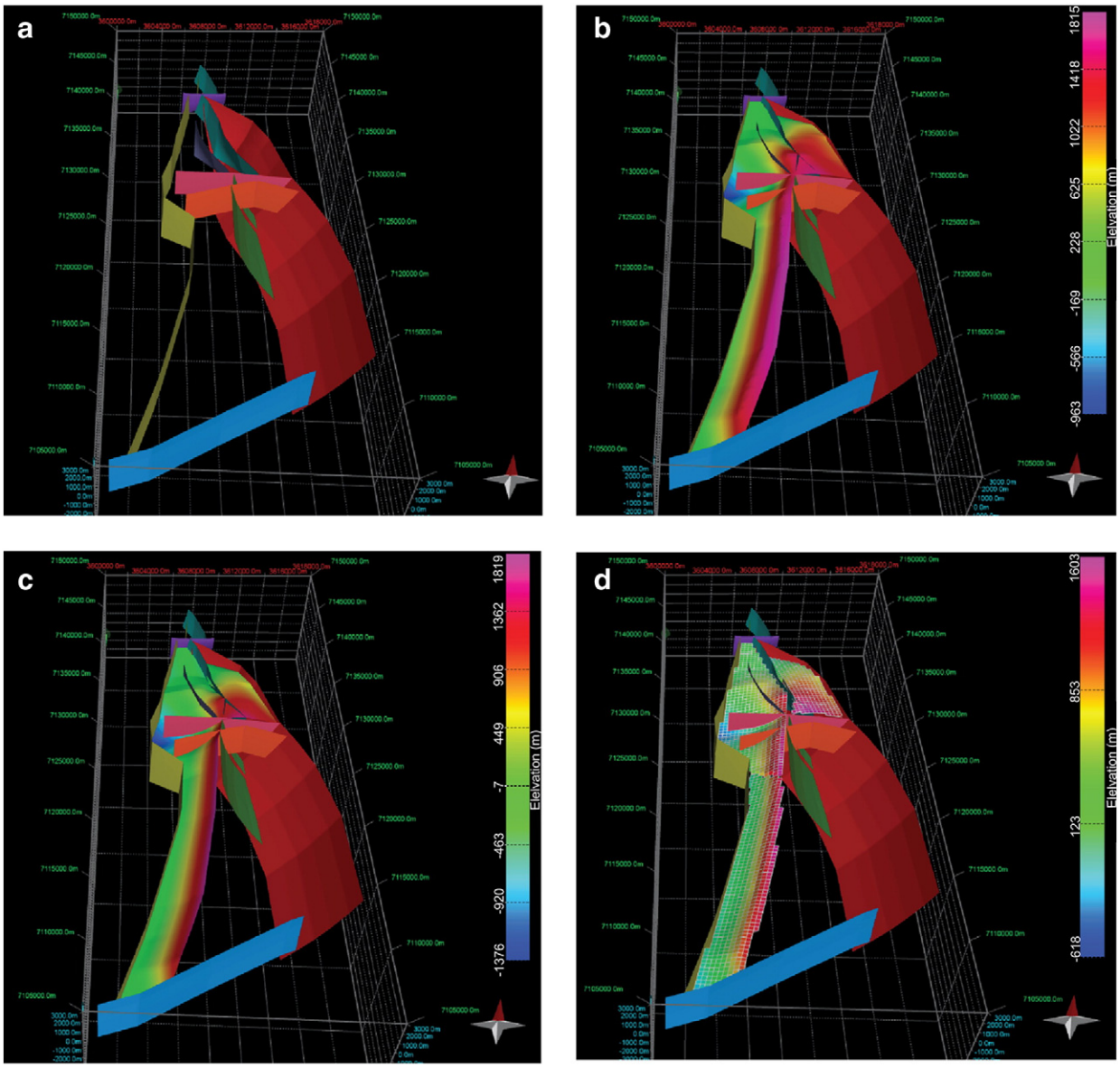

Fig. 5. Three-dimensional displays showing (A) the main interpreted fault planes, the contoured surface representing the top (B) and the bottom (C) of the reservoir, and (D) the geocellular volume of the reservoir. The 3-D volume represents the buried portion of the *Pirgua* Subgroup, whereas no volume was considered for its outcropping portion.

We identified in the field faults, generic fractures (e.g. defined as discontinuities with small aperture not sufficient to exclude a shear component during the opening, isolated weathered fracture) (Tavani et al., 2008), shear fractures, deformation bands, gypsum- and calcite-filled veins, and tectonic stylolites.

4.2.1. Southwestern backlimb

Along the south-western limb of the main *Sierra de La Candelaria* anticline, structural data were collected in two different sectors: *Anta Yaco* (north) and *Ceibal* (south) (Fig. 2A). In the *Anta Yaco* area, structural analyses were performed on *Anta*, *Yacoraite*, *Pirgua* and *Medina* Formations. Conversely, in the *Ceibal* area structural data were collected from the outcrops of *Pirgua* Subgroup and *Jesús María* Formations.

As a whole, the sedimentary succession cropping out along the backlimb strikes N–S, dipping about 40° to the W. The analyzed structures include generic fractures, shear fractures, veins and tectonic stylolites representing a spaced disjunctive cleavage produced by pressure solution.

Generic fractures occur in all the mechanical units exposed along the backlimb of the anticline. Poles to generic fractures show five main directions both in their present orientation and after bed rotation: N–S, E–W, NNW–SSE, ENE–WSW and WNW–ESE (Figs. 6A, B). N–S fractures are dominant and well visible in all the outcrops, and have generally high angle of dip (80°) both in the rotated and unrotated analysis. They are particularly abundant within the younger strata (*Jesús María* Fms.) with a constant spacing of about 30 cm and a length greater than 2 m; the aperture is from few centimeters up to 15 cm. E–W fractures occur in the strata of *Yacoraite* Formation and *Pirgua* Subgroup, in the area of *Anta Yaco* and *Ceibal*, respectively; they show a constant spacing of about 30 cm; their length varies from 30 cm to several meters and the aperture is mostly lower than 1 mm, but in some cases it reach a value of 3 mm such as in the strata of *Yacoraite* Formations.

NNW–SSE striking fractures, with high angle of dip, occur mainly in the strata of *Medina* and *Pirgua* Formations in the area of *Anta Yaco*. ENE–WSW and WNW–ESE generic fractures characterize the strata of *Pirgua* Subgroup in the *Ceibal* area.

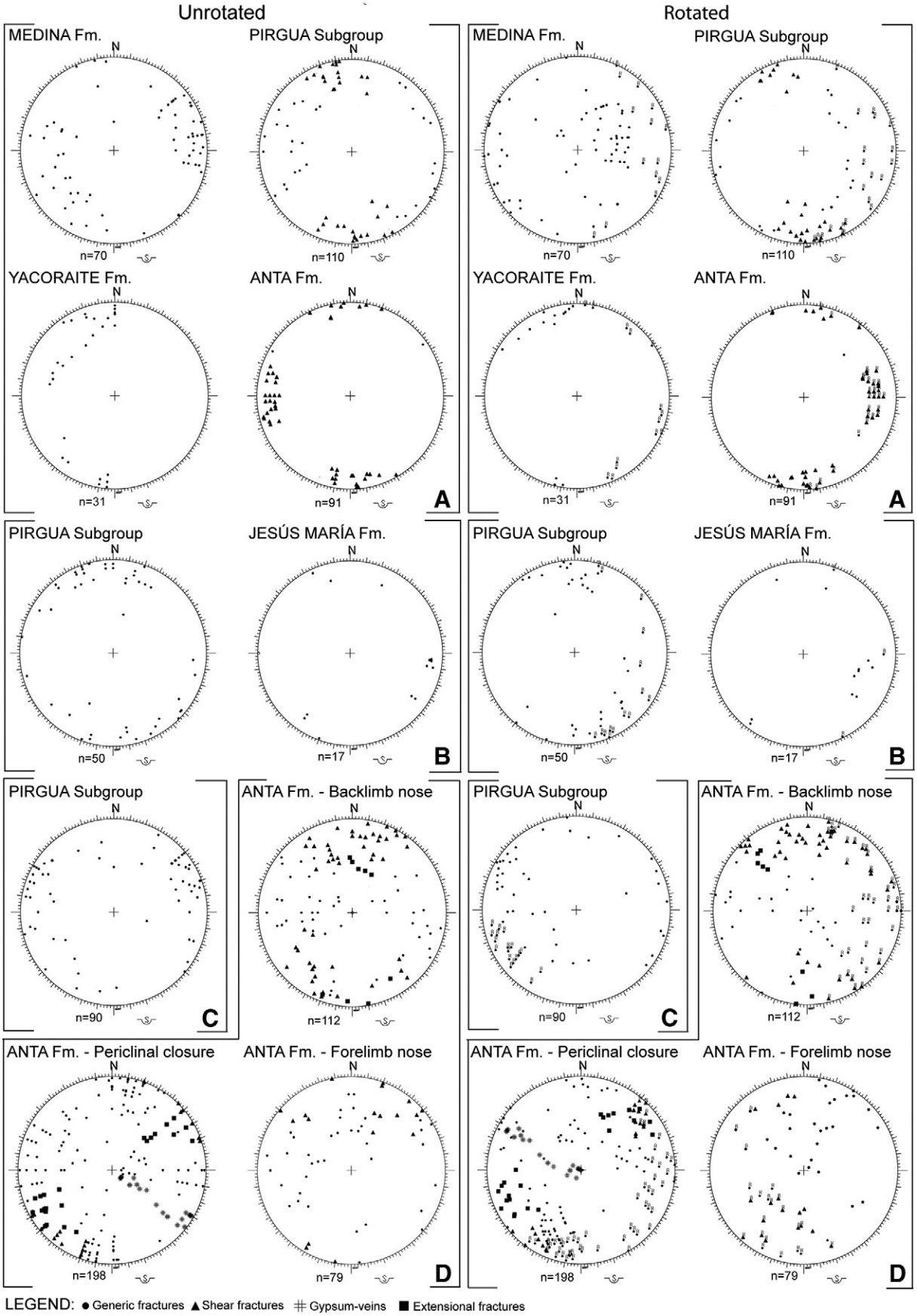

Fig. 6. Stereographic projections (Schmidt net, lower hemisphere) of the structural data collected in the (A) *Anta Yaco* and (B) *Ceibal* areas, (C) *Balboa* and (D) *Termas* anticlines.

In this latter area, calcite-filled veins are dominant in systematic sets striking along ENE–WSW and EW directions (Fig. 7A). They show a variable spacing ranging from several meters down to 30–40 cm; their thickness ranges from few millimeters to 2 cm.

Shear fractures were recognized in the strata of *Anta* and *Pirgua* Formations in the area of *Anta Yaco*. In the *Anta* Formation, they occur as a conjugate strike-slip systems striking NNW–SSE and E–W, steeply dipping and mutually cross cutting. The intersection line of these conjugate systems is parallel to the bedding suggesting a direction of contraction parallel to bedding dip (Fig. 7B). On the contrary, the strata of *Pirgua* Subgroup show a pervasive deformation characterized by E–W shear fractures with a right lateral component of motion and a constant spacing of about 30 cm (Fig. 7C); they are in accordance with the WNW–ESE shortening Andean direction (Marrett et al., 1994).

Stylolites trending N–S were observed in the strata of *Yacoraite* Formation (Fig. 7D). They occur normal to bedding and are interpreted as contractional structures.

Although the cross cutting relationship are not always consistent, N–S fractures are considered the younger one, because of their occurrence in the younger strata.

4.2.2. Northeast nose of Balboa anticline

Fractures data were collected from this portion of the anticline in the area of *Balboa* anticline, from the sandstones of *Pirgua* Subgroup (Fig. 6C). In this area, bedding strike rotates from N75°W to N20°W, as a consequence of the shape of the *Balboa* anticline (Fig. 2A).

Generic fractures, veins and deformation bands occur in the area. Poles to generic fractures are clustered around two broad maxima corresponding to roughly NE–SW and NW–SE trends, both in the rotated and unrotated analysis. These fractures are characterized by an average spacing of 35 cm. Subordinately, N–S generic fractures are also present. These fractures often mutually cross-cut, suggesting that they are essentially coeval.

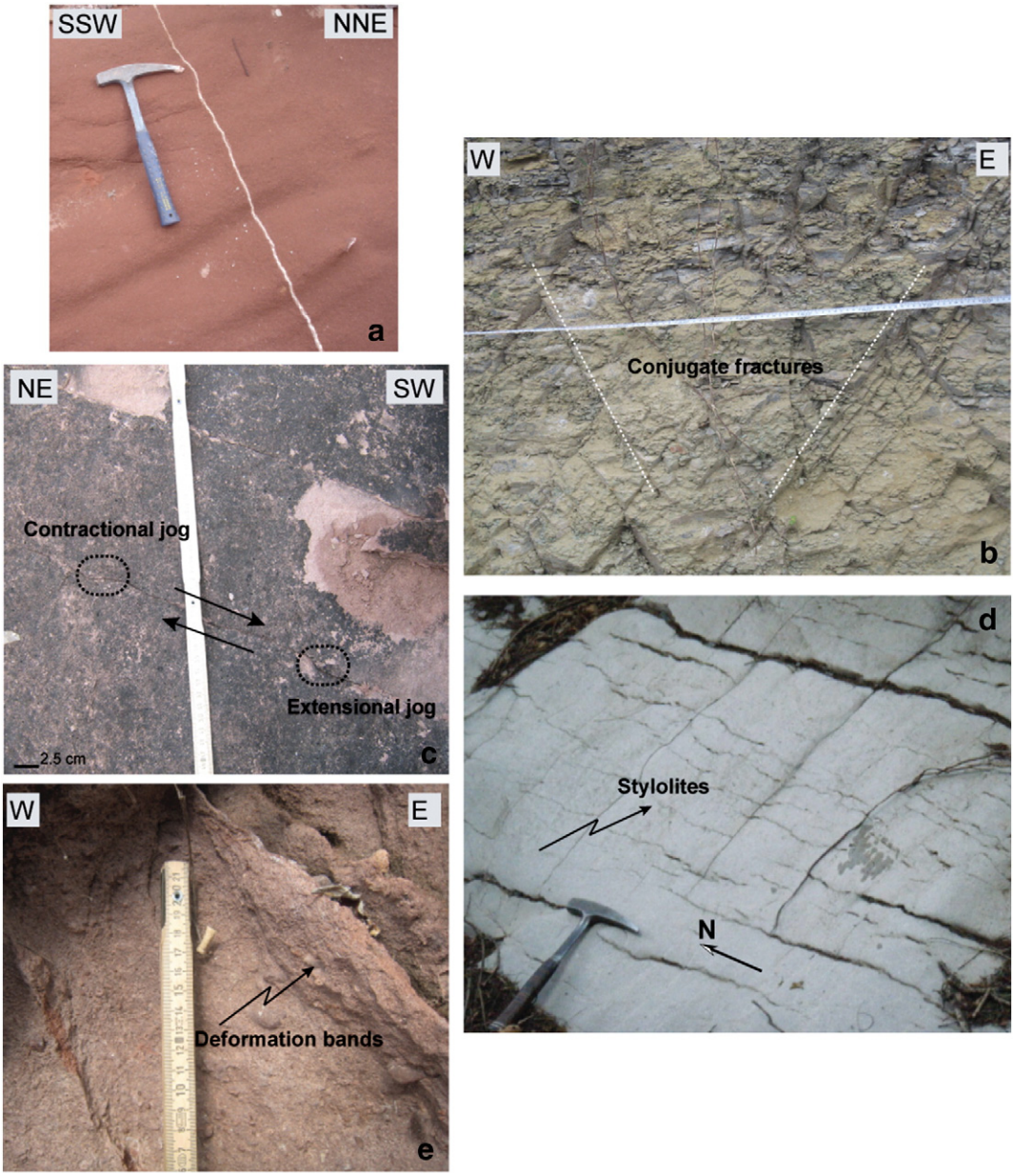

Fig. 7. Examples of the structural discontinuities observed in the field (A) Calcite-filled vein in the southwestern backlimb of the main anticline (*Pirgua* Subgroup). (B) Strike-slip conjugate fracture system in the backlimb of the main *Sierra de La Candelaria* anticline (*Anta* Formation). (C) Shear fractures in the backlimb of the main anticline (*Pirgua* Subgroup). (D) Stylolites oriented parallel to the bedding strike in the backlimb of the main anticline (*Yacoraite* Formation). (E) Deformation bands in the northeast nose of *Balboa* anticline (*Pirgua* Subgroup).

In addition, NW–SE and N–S fractures are often characterized by a positive relief with respect to the host rock, suggesting a high resistance to erosion. Their thickness is up to 5 mm and the higher compaction observed within, suggests the occurrence of deformation bands (Aydin and Johnson, 1978, 1983; Jamison & Stearns 1982; Underhill and Woodcock, 1987; Mair et al., 2000; Antonellini et al., 1994; Fossen and Hesthammer, 1997; Shipton and Cowie, 2001) (Fig. 7E).

Calcite-filled veins have the same directions NE–SW and NW–SE, and thickness variable from few millimeters up to 1.5 cm. Spacing is about 7 cm and 40 cm, respectively.

4.2.3. Northern nose of Termas anticline

In the area close to the *Hotel Termas*, the *Anta* Formation extensively crops out, and subordinately, *Jesús María* and *Guanaco* Formations. In detail, these two younger formations crop out in the eastern limb of the anticline, dip 15° to SE, and lay in unconformity on the older units (mainly *Anta* Formation) (Fig. 8). Brittle deformation is recorded only in the better cemented *Guanaco* beds, and consists of poorly developed, open fractures striking N075°E and N–S, likely compatible to the latest strike-slip motion along NNW–SSE lineaments and faults mapped in the *Hotel Termas* area.

In the same area, the well exposed strata of *Anta* Formation have different trends. In the backlimb nose of the anticline, bedding strikes ca. N–S and in the forelimb it strikes N030°W, dipping of about 60° in both cases. In the periclinal closure area, bedding strikes from N030°E, with a dip of about 50°, to N060°E with dip decreasing down to 30°. On the base of the qualitative analysis, we recognized on the field generic fractures, shear fractures and small faults, gypsum- and calcite-filled veins and deformation bands.

4.2.3.1. Backlimb. In the backlimb nose of the anticline, shear fractures striking NNW–SSE and E–W occur as a strike-slip conjugate system, compatible with the WNW–ESE shortening direction (Fig. 9A). The occurrence of NNW–SSE left-lateral faults suggests to interpret this association as Type I fracture array of Stearns (1968), indicating a direction of contraction parallel to dip direction of bedding, confirmed by the occurrence of synthetic Riedel shears making an angle of 15° with the main strike of these left–lateral faults.

Extensional ENE–WSW fault planes occur in the area. In some cases, they show transtensive kinematics with pitch values of about 40°.

Northward dipping, E–W striking normal faults and extensional fractures also occur in the area. Slickenlines on fault planes often show the superimposition of a dip-slip motion (slickenlines pitch between 70° and 120°).

A tighter packing of grains was observed in the area within fractures striking NNW–SSE and NE–SW suggesting deformation mechanisms typical of deformation bands. Shear fractures striking WNW–ESE and ENE–WSW cut-off these latter with a left-lateral kinematic (Fig. 10A).

In addition, generic fractures are recognized in the area with different orientations. In their present orientation (i.e. unrotated analysis), the dominant sets strike N–S and NE–SW, gently dipping (about 20°) to the east and south-east, respectively. The corresponding rotated analysis is characterized by a major maximum corresponding to N–S striking fractures that dip at high angle to the east. No shear or opened mode was observed in the field and the abutting relationship shows as NE–SW fractures post-dates the N–S trending ones.

4.2.3.2. Periclinal closure area. In the periclinal closure area where bedding strikes N60°E, extensional fractures striking NNW–SSE occur with a conjugate system of fractures dipping both to NE and to SW (mutually cross cutting). Therefore, they are interpreted as Type III fracture array of Stearns (1968), with the σ2 lying parallel to bedding. This interpretation is confirmed by the occurrence of normal faults striking sub-parallel to the fold axis that suggest extension parallel to bedding (Fig. 9B).

In the area of the *Hotel Termas*, where bedding strikes N30°E and dips to WNW, a decimetric shear zone occurs. It is composed by a pervasive system of normal and transtensive fault planes. These fault planes strike N30°W and they are sub-vertical or highly dipping mainly towards the eastern quadrants. Slickenlines on fault planes have azimuth to N005°. The architecture of the damaged fault zones consists of main shear surfaces and subsidiary Riedel planes striking N50°W with slickenlines striking N20° and N290°. Furthermore, in this shear zone is also present a spaced cleavage folded into Z-shaped folds with steeply plunging axes and asymmetry suggesting a left-lateral motion in correspondence to the major fault planes (Fig. 9C). Calcite infillings often occur in correspondence to the transtensive WNW-ESE fault planes.

In addition, in this area, in correspondence to the thick pelitic layer that characterized *Anta* Formation, three families of gypsum-veins occur (Fig. 9D). They strike NNE–SSW dipping to NW both steeply and gently. Gypsum veins steeply dipping and sub-parallel to bedding are characterized by gypsum crystals both orthogonal and oblique with respect to the fracture walls. Both of these fill types seem to be compatible to shear parallel to bedding, developed during a flexural slip process. The first one, extensional, suggests a first decompression of strata (σ3 normal to bedding, σ1 horizontal), related to the first phase of folding, followed by shear along bedding (flexural slip). A third family of gypsum veins is gently

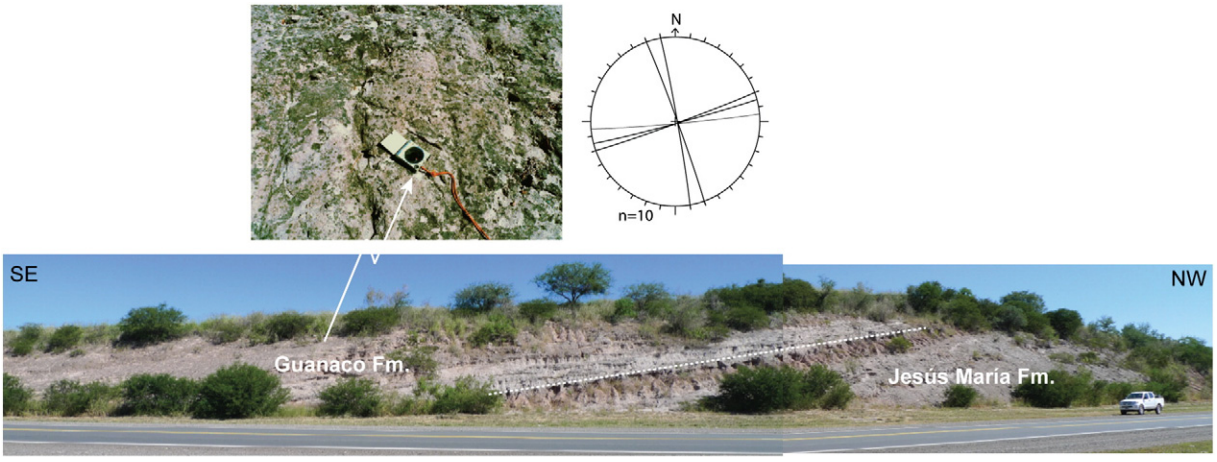

Fig. 8. *Guanaco* and *Jesús María* Formations cropping out with a visible unconformity separating them. The stereoplot (Schmidt net, lower hemisphere projection) shows the corresponding structural data set collected on the strata of *Guanaco* Formation.

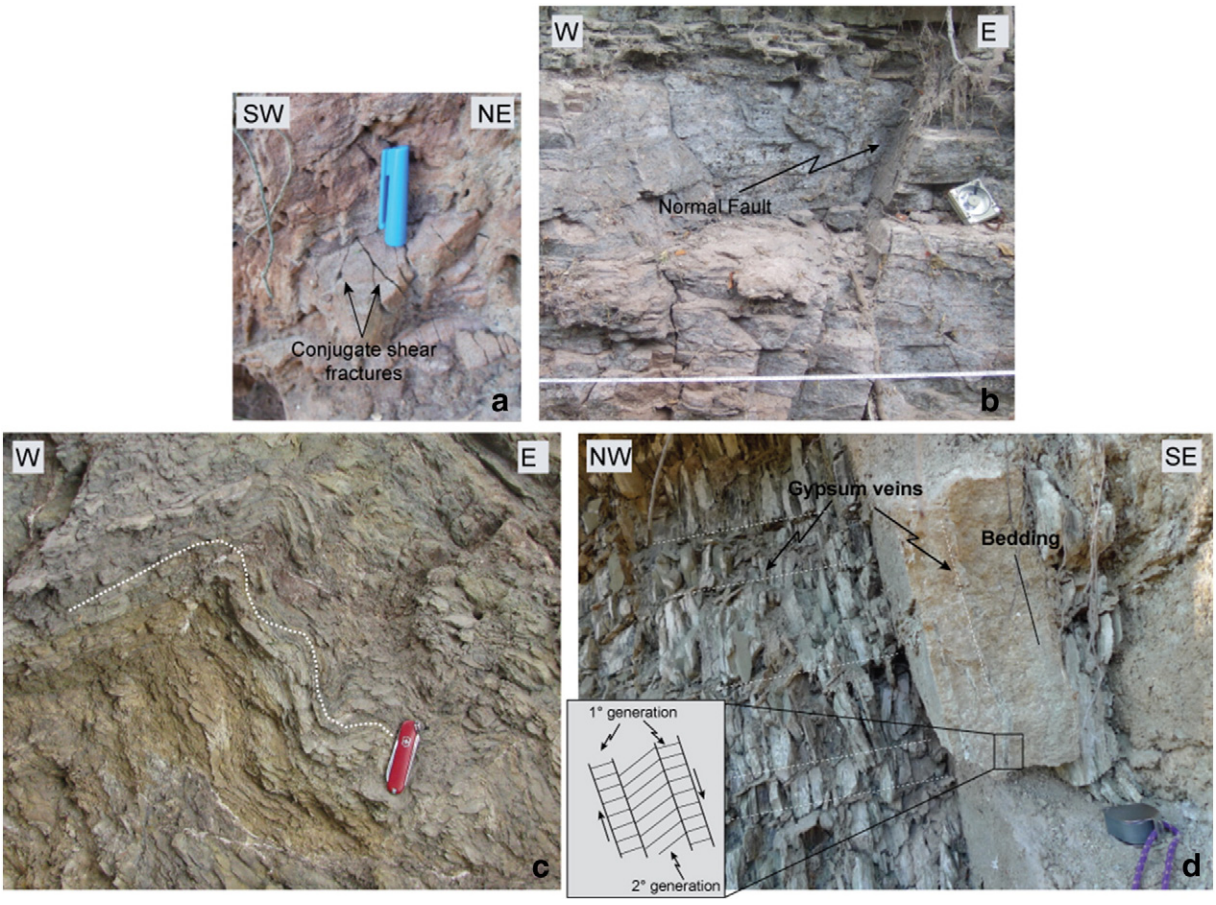

Fig. 9. Examples of the structural discontinuities observed on the strata of *Anta* Formation in correspondence to the *Termas* anticline: (A) Conjugate shear fractures (backlimb nose). (B) Longitudinal normal fault (periclinal closure area). (C) Spaced cleavage folded into Z-shaped folds with steeply plunging axes (periclinal closure area). (D) Three families of gypsum veins (periclinal closure area). In the square, two families sub-parallel to bedding characterized by gypsum crystals orthogonal and oblique with respect to the fracture walls.

dipping and at high angle to bedding. It is characterized by gypsum crystals oblique of about 30° with respect to the fracture walls indicating a sense of shear with top to NE. This latter family overprints the other sets and could be related to the final phase of compression (shear planes cutting the fold limbs).

Generic fractures are also frequent in the area. Where bedding strikes N30°E, they occur with a strike WNW–ESE and E–W. They are often open, with an aperture of about 3 mm, and often occur in association with gypsum-veins described above; abutting relationship shows as generic fractures striking WNW–ESE cut the system of gypsum-veins (Fig. 10B). Generic fractures striking N–S and steeply dipping to both directions represent the most frequent set where bedding strike N060°E. Even though no open mode was detected in the field, in some cases, the occurrence of calcite-filled veins with the same trend suggests a tensile origin for this fracture set.

4.2.3.3. Forelimb. Generic fractures are organized in this area in three main trends striking E–W (dipping to south at low angle) and NW–SE (dipping to south-west at a high angle). Subordinatley, a N–S fracture trend occurs. It dips to the east at low angle.

Deformation bands striking WNW–ESE and ENE–WSW were recognized in the area. Shear fractures striking WNW–ESE and ENE–WSW occur in the area with a right- and left-lateral kinematic, respectively (Fig. 10C).

5. Reservoir Discrete Fracture Network model

We built a DFN model within the 3D volume of the geothermal reservoir. It represents the merge of twenty-four stochastic DFN models generated for each fracture set recognized in the different portions of the anticline in correspondence to the reservoir outcrops. In the area of *Termas* anticline, where the reservoir does not outcrop, fracture data collected from the strata of *Anta* Formations are considered to model the fracture network in the buried portion of the reservoir.

Accordingly, fracture dataset was divided into six sets that can be grouped into longitudinal (set I), transverse (sets II) and oblique (IA, IB, IIA and IIB) with respect to the fold axis. In detail:

- Set I includes N30°W±10° fractures, striking sub-parallel to the fold axis;
- Set IA and Set IB include fractures striking N60°W ± 10° and N–S ± 10°, respectively;
- Set II includes fractures striking N60°E ± 10°, transverse to the fold axis;
- Set IIA and Set IIB includes fractures striking N30°E ± 10° and E–W ± 10°, respectively.

The frequency of the different fracture sets varies through the different formations and along the anticline (Fig. 11).

In order to perform the fracture modeling in the reconstructed reservoir volume, the software requires some initial input parameters concerning the fracture intensity, the mean orientation for each set of fractures (obtained by the fracture set orientation analysis), and the statistical fracture-size distribution. The required input parameters were calculated for each fracture set from the scan-line surveys carried out on the outcrops of reservoir and cap rocks in different portions of the anticline (Table 2).

Fracture intensity represents the amount of fractures per measure unit, and can be expressed by the number of fractures per

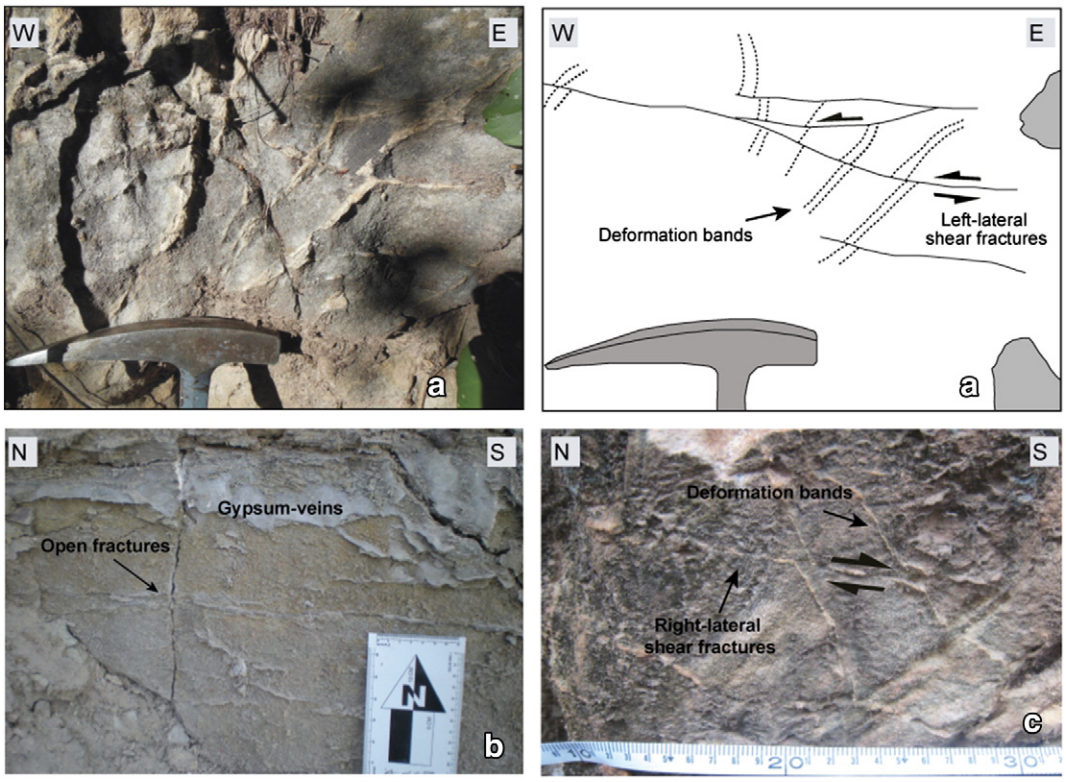

Fig. 10. Examples of structural cross-cutting relationships observed on the strata of *Anta* Formation in correspondence to the *Termas* anticline: (A) Left-lateral shear fractures (backlimb nose). (B) Open fractures cutting gypsum veins (periclinal closure area). (C) Shear fractures offset deformation bands with a right-lateral motion (forelimb nose).

volume (parameter P30), the fracture length per volume (P31), or the fracture area per volume (P32) (Dershowitz and Herda, 1992). In particular, the software used during this modeling generates DFN models using two of these intensity parameters, the P30 and P32 values.

In the present work, we have used the P32 intensity parameter calculated from the number of fractures per length of scan-line measured during the fieldwork for each fracture set. Fracture frequency value, derived from scan-line surveys and corrected by Terzaghi for removing sampling bias, can be used as roughly equivalent to the 3D fracture intensity (m^2/m^3) (Priest, 2004).

Fracture length distribution and fracture orientation are the other two important input parameters for the generation of the DNFs. Fracture orientation was computed through the Fisher model that provides average dip, dip azimuth values and a concentration parameter (K) for orientation of each fracture set (Table 2). Analysis of fracture lengths measured in the field show a normal cumulative size distribution.

The last parameter requested by the software to complete the modeling phase is the aperture value of each fracture set. It represents an important parameter as it has a large influence on the calculated permeability of the model by the "cubic law" (Louis, 1969; Kranz et al., 1979; Tsang and Witherspoon, 1981; Fetter, 1993). In fact, according to the so-called parallel plate model (Snow, 1965; Witherspoon et al., 1980) the flow rate along a fracture is related to the cube of the aperture and thus permeability K_j of a single fracture is given by:

$$Kj = \frac{(Ha)^2}{12} \quad (1)$$

where H_a represents the hydraulic aperture of the fracture.

Because the permeability of deformation bands can be one or more orders of magnitude less than the matrix permeability (Aydin, 2000; Sternlof et al., 2004), and permeability of other structural discontinuities, depending on their aperture, can be several orders of magnitude greater than matrix permeability, the combined effect of these structures on subsurface flow can be complex and substantial. For this reason, the deformation bands recognized in the outcrops of *Pirgua* Subgroup in the area of *Balboa* anticline were not included in the fracture modeling, since they are interpreted to reduce the reservoir permeability acting as barriers to flow (reservoir type 4 of Nelson, 1992).

Moreover, for the other fracture types we have considered aperture value as proportional to the trace length of fractures basing on the non-linear, square root power-law distribution between aperture and length, proposed by Olson (2003):

$$D_{max} = \alpha L^{0.5} \quad (2)$$

where D_{max} is the maximum (shearing) displacement along the fault/fracture, L the length and α a proportionality coefficient:

$$\alpha = \frac{K_{Ic}(1-\nu)2}{E}\frac{\sqrt{8}}{\sqrt{\pi}} \quad (3)$$

including the fracture toughness K_{Ic}, Poison's ratio ν, and Young's modulus E, all material specific constants of the host rock.

We do not consider a linear correlation between aperture and length since Olson (2003) demonstrated that an exponent greater than 0.5 in Eq. (2) could result from post-jointing relaxation or other secondary effects, whereas an exponent of 0.5 is related to a constant fracture toughness, which describes the ability of a rock containing fractures to resist further fracturing (Olson, 2003; Schultz et al., 2008).

Once calculated the different parameters for the six fracture sets, we have considered their variability across the anticline. To represent this in the DFN model, the entire volume was divided in different small volumes, one for every different fracture density value considered within the anticline. In fact, on the base of the structural analysis carried at

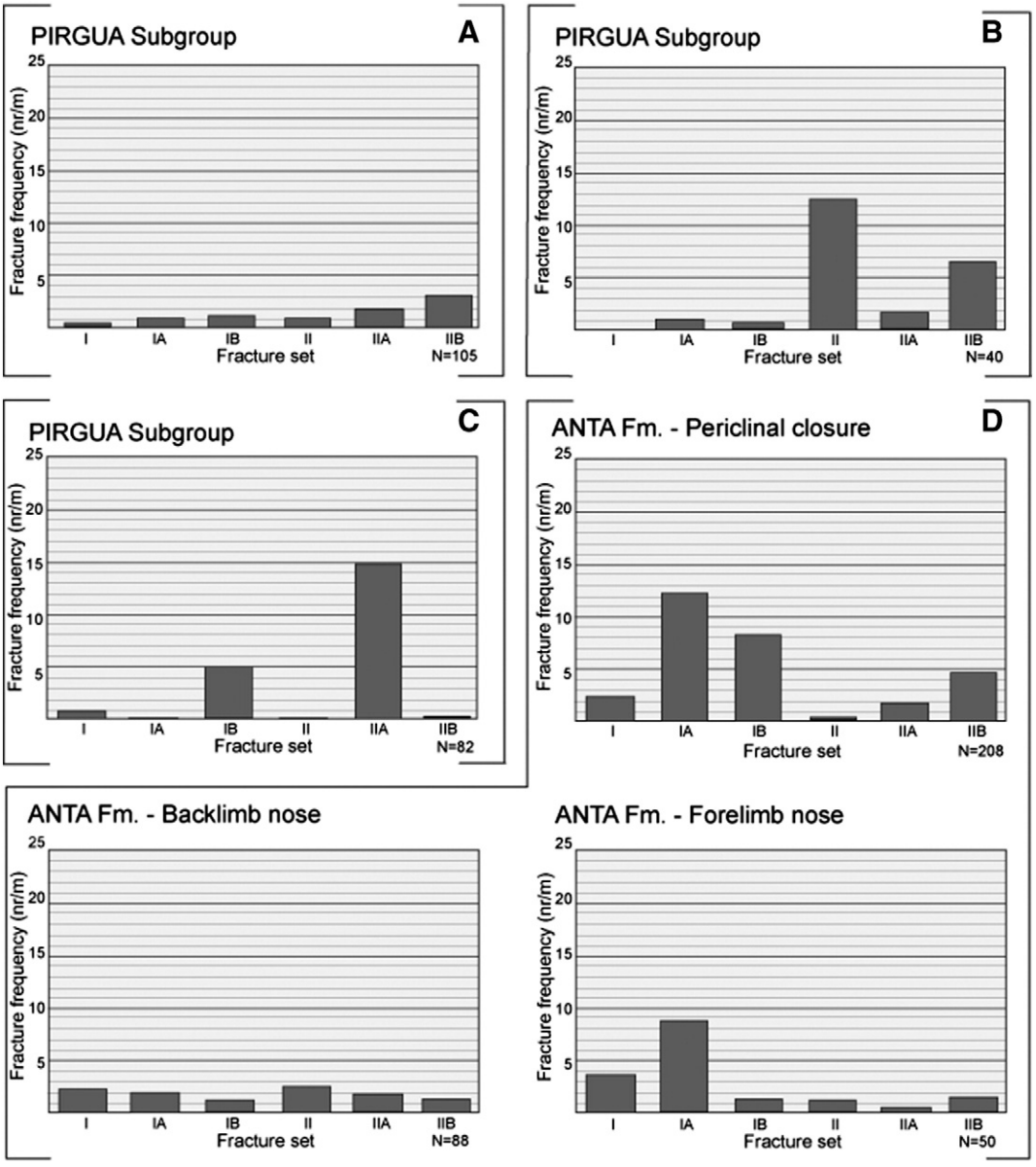

Fig. 11. Histograms showing the fracture frequency values for each fracture set computed for the reservoir and cap rock in the (A) *Anta Yaco* and (B) *Ceibal* areas, (C) *Balboa* and (D) *Termas* anticlines. Fracture frequency values are calculated from the number of fractures per unit length of scan-line measured during this specific survey for each fracture set and corrected by Terzaghi for removing sampling bias.

the outcrop scale we have recognized several different areas along the anticline characterized by different deformation intensity: *Balboa* and *Termas* anticlines, *Anta Yaco* and *Ceibal* areas (see paragraph 4.2 for details).

Finally, we have generated twenty-four DFN models, six for every area (Fig. 12), which formed the total one. It allowed to calculate the fractured volume affecting the reservoir resulting of 0.02 km^3 (Table 3). It is considered as the profit volume that enhances fluid flow.

6. DFN upscaling

The upscaling process converts the Discrete Fracture Network model to equivalent continuum medium of the required properties distributed over a grid. Therefore, the volume referred to the reservoir rock was converted in a grid formed by 2506 cubic cells with a side of 300 m. For each grid cell, a permeability tensor based on the DFNs was computed using the geometric methodology proposed by Oda (1985). The calculation of the permeability tensor that the fracture modeling module performs is therefore geometric, and done on the base of all fracture fragments that belong to each cell in the geocellular volume. Therefore, the contribution to the permeability of each fracture depends on the clipped fracture polygon area, the aperture dimension, and the orientation of the fracture.

Table 3 shows the values of permeability tensor computed by the software for the twenty-four DFNs performed.

In detail, permeability shows the highest values (between 8 and 10 mD) in correspondence to the *Termas* and *Balboa* anticlines and in the area of *Ceibal*, where fractures are characterized by the highest values of frequency. The comparison among permeability values due to the different fracture sets shows that the highest values are due to the oblique fractures belonging to set IB and IIA in correspondence to the two minor anticlines, and to the transverse fracture set II in the area of *Ceibal*. Accordingly, these fracture sets show high values of aperture and frequency. On the contrary, the lowest values of permeability occur along the backlimb of the main anticline, in the *Anta*

Table 2
Parameters calculated for the six fracture sets in the four measurement areas of the anticline. Length values (mean and standard deviation) were obtained by distribution analysis performed with EasyFit. All fracture sets show a normal distribution except for fracture set II in the area of Balboa anticline that shows a constant distribution. Mean principal plane includes the average values of dip and dip direction obtained with the Fisher method implemented in Move 2013 (Midland Valley).

	Set I	Set IA	Set IB	Set II	Set IIA	Set IIB
Anta Yaco area						
P32	1.03	1.56	4.03	7.05	10.03	9.57
Aperture (mm)	0.50	0.65	0.77	0.59	0.50	0.53
Mean length (m)–std. dev. (m)	0.55–0.26	0.79–0.50	0.82–0.84	0.72–0.37	0.59–0.32	0.64–0.27
Mean principal plane (°)	79/243	67/27	59/94	72/329	72/296	75/76
Fisher dispersion (K value)	83.29	18.00	17.83	33.54	27.36	37.51
Ceibal area						
P32	0.27	1.25	0.99	12.74	2.43	7.96
Aperture (mm)	0.50	0.80	0.10	1.00	0.79	0.55
Mean length (m)–std. dev. (m)	0.55–0.26	0.98–0.91	0.04–0.03	1.18–1.65	0.81–0.94	0.83–0.18
Mean principal plane (°)	79/243	86/26	77/280	88/150	88/309	56/176
Fisher dispersion (K value)	83.29	1.30	109.30	1.23	2.13	1.50
Balboa anticline						
P32	1.00	0.27	5.16	0.06	14.96	0.22
Aperture (mm)	0.84	0.72	0.79	0.35	0.89	0.59
Mean length (m)–std. dev. (m)	1.09–0.85	0.81–0.60	1.17–0.67	0.33	0.91–1.09	0.62–0.37
Mean principal plane (°)	76/239	55/210	73/260	65/150	80/120	72/171
Fisher dispersion (K value)	42.00	65.47	46.56	*Constant*	45.55	34.70
Termas anticline						
P32	2.03	1.83	9.19	7.11	24.99	9.79
Aperture (mm)	0.70	0.69	0.79	0.56	0.74	0.57
Mean length (m)–Std. dev. (m)	0.82–0.56	0.80–0.55	0.99–0.75	0.52–0.37	0.75–0.71	0.63–0.33
Mean principal plane (°)	77/241	61/210	66/260	68/329	75/120	73/171
Fisher dispersion (K value)	62.65	64.37	46.56	35.00	45.55	34.70

Yaco area (2 mD). In this latter area, the highest values are due to the fracture sets IB, II and IIB that are the most frequent and open.

Fig. 13 shows the distribution of the permeability inside the geocellular volume. Changes in the different directions (i.e. xx, yy, xy, xz, yz, zz) are in agreement with the anisotropy of the distribution of the fractures orientation.

7. Discussion

7.1. Tectonic interpretation of the deformation sequence

The best starting point in order to assess the reservoir quality for exploration programs consists in the elaboration of a reliable tectonic

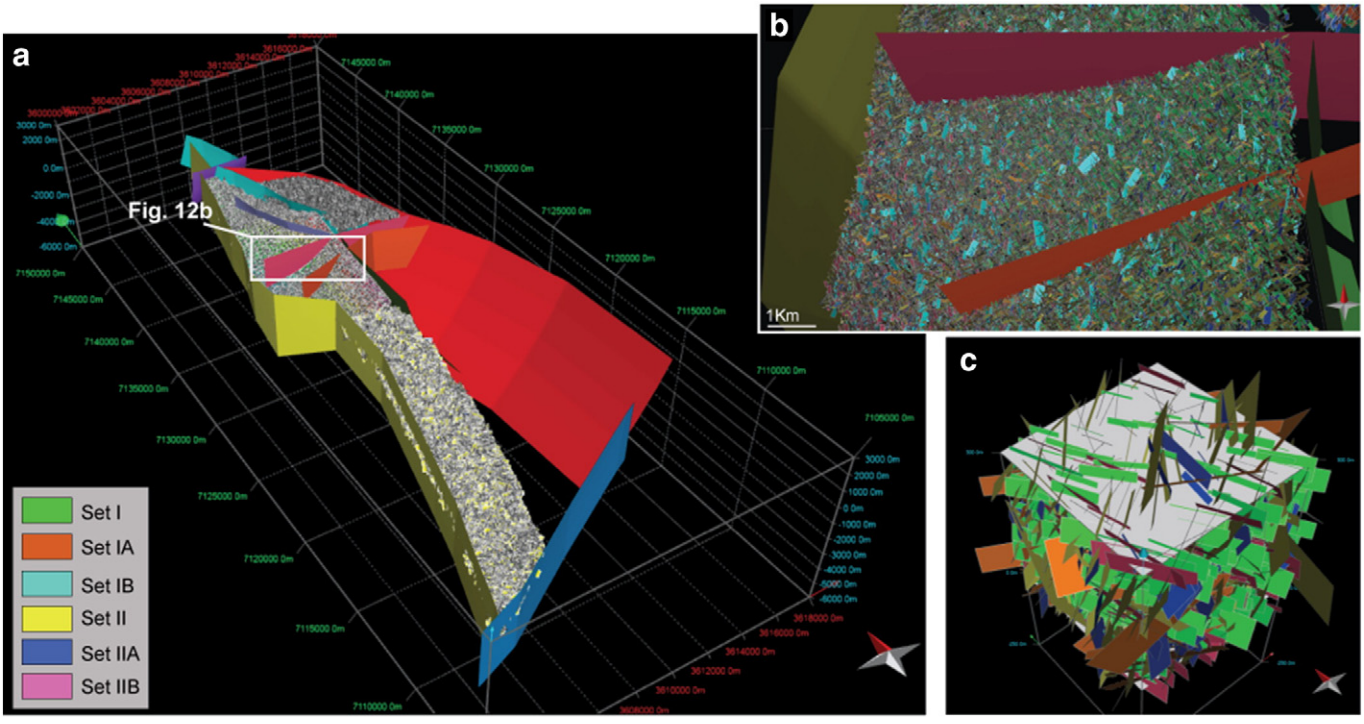

Fig. 12. (A) Three-dimensional fracture model reconstructed inside the geocellular volume of the reservoir. (B) Detail of the 3-D fracture model shown in panel a. (C) Top view of the grid cell illustrating the trend of the six main sets of fractures.

Table 3
Permeability tensor (mD) computed for each fracture set and for the fracture network (all fracture sets together) in the four areas of the anticline. Fracture volume was obtained by the software on the base of the reconstructed DFN models considering aperture, length and density of each fracture set.

	Set I	Set IA	Set IB	Set II	Set IIA	Set IIB	Fracture network
Anta Yaco area							
Permeability (mD)	0.11	0.48	1.85	1.22	1.11	1.21	5.98
Fracture volume (km^3)	8.3E-05	2.2E-04	5.7E-04	6.8E-04	8.5E-04	8.7E-04	3.3E-03
Ceibal area							
Permeability (mD)	0.04	0.58	0.10	10.38	1.36	0.76	13.22
Fracture volume (km^3)	1.2E-05	9.3E-05	4.2E-05	1.2E-03	2.2E-04	3.5E-04	2E-03
Balboa anticline							
Permeability (mD)	0.67	0.17	1.89	0.002	8.69	0.06	11.48
Fracture volume (km^3)	6.3E-05	1.7E-05	2.9E-04	1.6E-06	1.1E-03	8.9E-06	1.5E-03
Termas anticline							
Permeability (mD)	0.69	0.65	4.49	1.17	9.78	1.60	18.37
Fracture volume (km^3)	2.9E-04	2.9E-04	1.7E-03	8.3E-04	4.1E-03	1.1E-03	8.3E-03

model of the studied geothermal field. It helps making predictions about lithology, faulting, and fluid flow in and out of the reservoir. Moreover, it provides a robust data set for the interpretation of faulting and placement of wells. In particular, the formation and evolution of natural fractures are closely related to the deformation history of the host rock.

The kinematic evolution and timing of the studied anticline is deciphered by analyzing (1) the structural relationships with the faults mapped in the area, (2) the geometry of the different stratigraphic units, and (3) the structural data collected at the outcrop scale.

In general, the analysis of the deformation pattern shows that both the attitude and kinematic of most tectonic structures are consistent with two main deformation phases, that can be traced throughout Cretaceous to present day: 1. extension and 2. positive inversion and folding. Data at the outcrop scale allow refining the timing of deformation of event 2 into early, intermediate and mature sub-stages.

Extension due to Cretaceous rifting is recorded by an increase in total thickness (from 400 to 450 m) and bed thickness (from less than 1 m up to 5–6 m) of the syn-rift *Pirgua* Subgroup. Moreover, their clastic facies

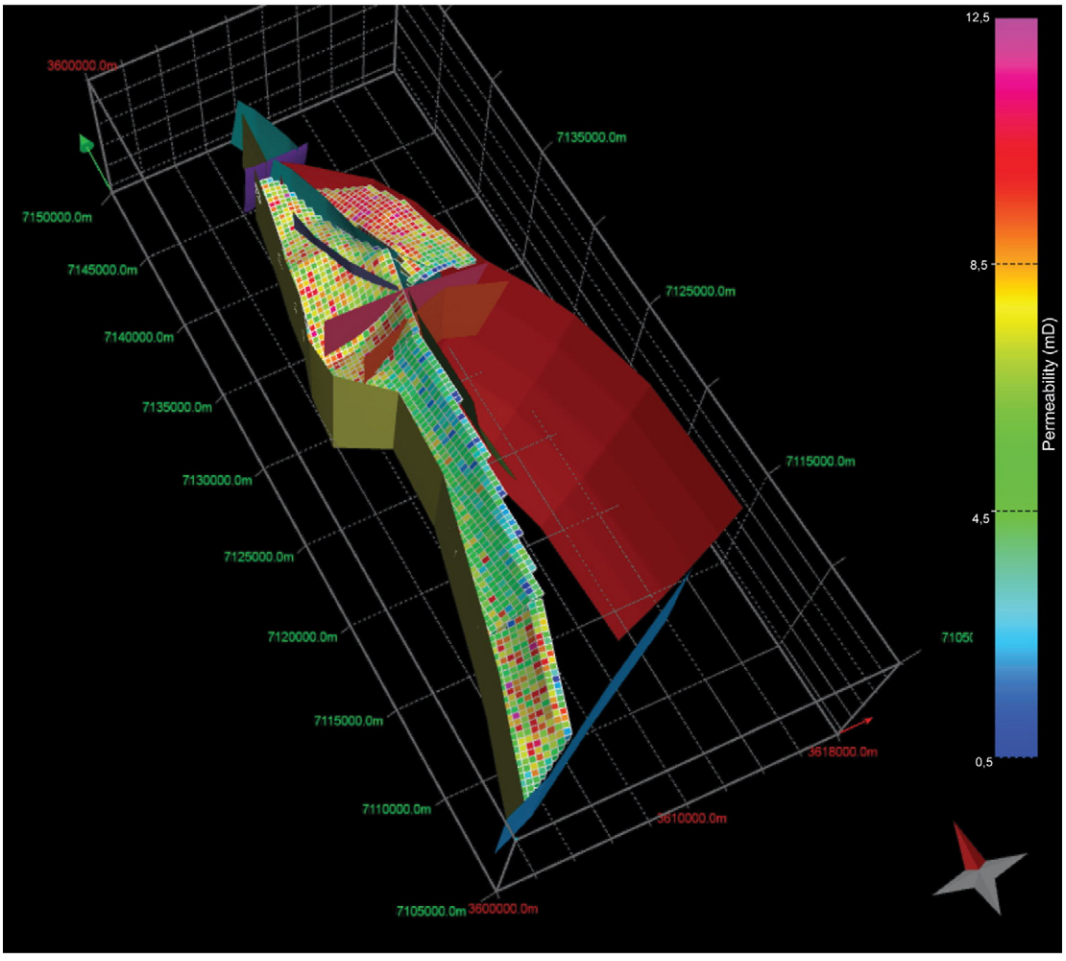

Fig. 13. Color map showing the distribution of permeability inside the reservoir (see text for detailed explanation).

evolves from mainly arenitic to mainly conglomeratic moving from the area of *Anta Yaco* to the area of the *Balboa* anticline. This facies and thickness lateral variation indicates that the area of the *Balboa* anticline was proximal to a syn-sedimentary normal fault that limited the succession to the east, in agreement with the syn-rift paleogeography proposed by Marquillas et al. (2005). This evidence supports the hypothesis that the fault that borders the *Sierra de La Candelaria* to the east started as normal fault during the Cretaceous rifting process and was inverted during the Cenozoic tectonic phase (in agreement with Iaffa et al., 2013) (Fig. 14A). The same high-angle inverted fault shows a left strike-slip kinematic component compatible to the latest Andean regional WNW–ESE shortening direction (also in agreement with Marrett et al., 1994). Furthermore, it is responsible of the uplift of the *Sierra de La Candelaria* structure, deformed in a N–S trending hangingwall anticline (Moreno Espelta et al., 1975; Seggiaro et al., 1997).

In the early stage of inversion, deformation is recorded mainly at the outcrop scale by:

- gypsum extensional veins striking NNE–SSW, steeply dipping and at low angle to bedding in the pelitic strata of *Anta* Formation. They indicate the initial stage of folding under overpressure condition (Shearman et al., 1972; Sibson and Scott, 1998; Gustavson et al., 1994);
- N–S-striking stylolites in the strata of *Yacoraite* Formation.

In the intermediate stage of inversion, the deformation in the hangingwall was accommodated by growing of the regional anticline and activity of a N–S trending backthrust bordering the western limb of the anticline. This last is likely to be connected at depth to the inverted fault (Fig. 14B). At this stage, the anticline development was accompanied by a series of related syn-folding features at the outcrop scale. In the southern sector of the anticline, along its western limb in the area of *Anta Yaco* and *Ceibal*, they are represented by:

- NNW–SSE and E–W striking conjugate strike-slip fractures observed in the strata of *Anta* Formation;
- E–W shear fractures with a right-lateral kinematic, mainly occurring in the strata of *Pirgua* Subgroup. They are in accordance with the WNW–ESE shortening direction;
- E–W and WNW–ESE striking generic fractures recorded in the strata of *Yacoraite* Formation and *Pirgua* Subgroup, in the area of *Anta Yaco* and *Ceibal*, respectively.

In the northern nose of *Termas* anticline where *Anta* Formation crops out, syn-folding features are represented by:

- Shear veins in gypsum bearing pelites of *Anta* Formation. They testify flexural slip on both limbs;
- NNW–SSE and E–W conjugate shear fractures occurring in the backlimb. They are interpreted as Type I fracture array of Stearns (1968);
- N–S-trending joint and calcite filled veins in the periclinal closure area. They record an extension sub-parallel to the fold axis trend;
- NNW–SSE striking conjugate system of extensional fractures recorded in the periclinal closure area. They are interpreted as Type III of Stearns (1968);
- WNW–ESE striking deformation bands and shear fractures with a right-lateral kinematic occurring in the forelimb nose of the anticline;
- WNW–ESE and E–W generic fractures in the periclinal closure area and in the forelimb nose of the anticline.

In the late stage of inversion, the northern portion of the regional anticline was dissected by a NNW–SSE oblique fault plane. It dissects the main anticline enhancing the development of the *Balboa* and *Termas* minor anticlines, in agreement with Barcelona et al. (2014). The occurrence of this fault characterized by reverse dip-slip and left-lateral strike-slip components defines a positive flower-like structure with associated minor NW–SE faults. These latter splay off the NNW–SSE fault plane in the sense of Riedel shears with a left-lateral strike-slip transtensional kinematic (Fig. 14C). Different meso-structures, characterizing the outcrops of *Anta* Formation in correspondence to the *Termas* anticline, testify the strike-slip kinematic along these faults:

- NNW–SSE left-lateral faults and the associated Riedel shears occurring in the periclinal closure area;
- NNW–SSE striking deformation bands recorded in the backlimb of the anticline;
- N–S, NW–SE and NE–SW generic fractures occurring in the backlimb and in the forelimb of the anticline.

In the younger strata of the *Guanaco* Formation (*Jujuy* Subgroup), NS and ENE–WSW trending fractures are compatible to the latest strike-slip motion along NNW–SSE lineaments and faults mapped in the area of the *Hotel Termas*.

A strike-slip kinematic is also recorded in the strata of *Pirgua* Subgroup, in the area of *Ceibal* and *Anta Yaco*, and in correspondence to the *Balboa* anticline. In detail, in this latter area, NW–SE and N–S striking deformation bands and N–S, NW–SE and NE–SW generic fractures testify the occurrence of this kinematic. On the contrary, the left-lateral strike-slip fault trending NE–SW and off-setting the stratigraphic succession in the area of *Ceibal*, is better recorded at the outcrop scale from fractures striking E–W, NE–SW and WNW–ESE. The map view analysis suggests that this fault occurred after fold development. Furthermore, the occurrence of the highest frequency of the fracture sets related to the NE–SW strike-slip fault in the strata of *Pirgua* Subgroup suggests that this fault was active after the deposition of the units of *Salta* Group and before the deposition of *Jesús María* Formation in which they are not observed. At the same time, the ENE–WSW left-lateral shear fractures occurring along the limbs of *Termas* anticline are correlable to this deformative event.

Later on, in the late stage of inversion, in the central and northern portions of the structure, E–W trending normal faults dipping both to the north and to the south dissect main compressive and transpressive deformation (Fig. 14D). These faults are interpreted to occur in the final stage of the regional fold growing generated by an extension perpendicular to fold axis on the base of cross-cut relationships. This latter event chronology differs from Iaffa et al.'s reconstruction (2013) that considers these faults as passively inherited Cretaceous normal faults. At the outcrop scale, the E–W conjugate system of extensional fractures and the ENE–WSW and E–W normal faults occurring in the strata of *Anta* Formation in correspondence to the backlimb nose of *Termas* anticline are interpreted to reflect this final stage of the folding process.

The original results presented in this paper allow us to propose a kinematic evolutionary model of the area in an integrated framework that was missing in the past literature. Previous structural investigations of the area provided a kinematic interpretation invoking only a generic model of positive inversion based on structural pieces of evidence collected at regional scale (Moreno Espelta et al., 1975; Cristallini et al., 1997; Seggiaro et al., 1997; Iaffa et al., 2011; Iaffa et al., 2013). On the other hand, the new interpretation takes into account a refined

Fig. 14. Schematic interpretation of the kinematic evolution of the *Sierra de La Candelaria* anticline. It shows the (A) early, (B) intermediate and (C, D) mature stages of the deformation that produced the regional anticline. (E) A scheme of the different mesostructures associated to the early (pink color), intermediate (blue) and mature deformation stages (green and orange) of the anticline. See text for details.

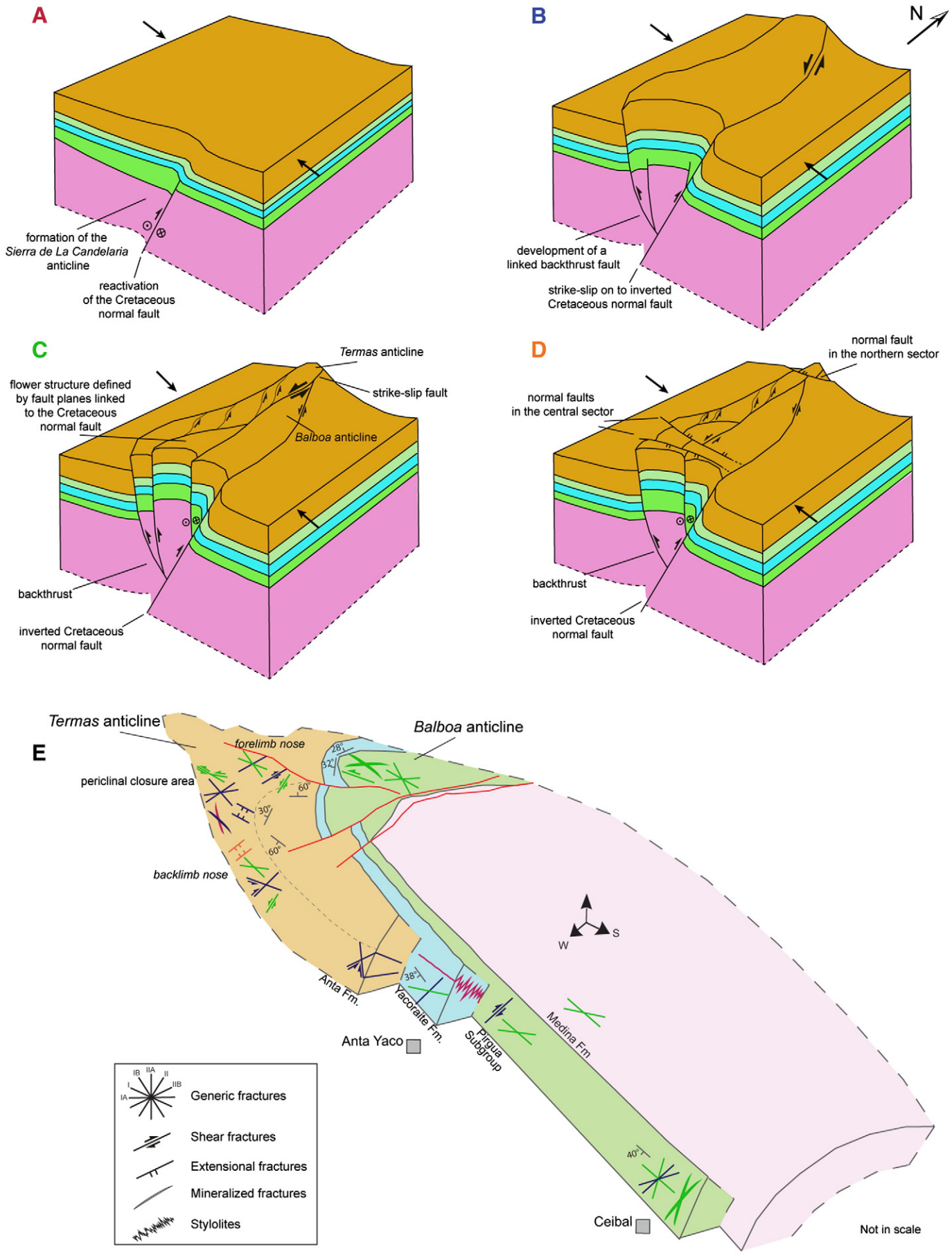
A
formation of the
Sierra de La Candelaria
anticline
reactivation
of the Cretaceous
normal fault
B
N
development of a
linked backthrust fault
strike-slip on to inverted
Cretaceous normal fault
C
Termas anticline
flower structure defined
by fault planes linked
to the Cretaceous
normal fault
strike-slip fault
Balboa anticline
backthrust
inverted Cretaceous
normal fault
D
normal fault
in the northern sector
normal faults
in the central sector
backthrust
inverted Cretaceous
normal fault
E
Termas anticline
Balboa anticline
forelimb nose
periclinal closure area
backlimb nose
28°
32°
60°
30°
60°
38°
W
S
Anta Fm.
Yacoraite Fm.
Anta Yaco
Pirgua
Subgroup
Medina Fm
40°
Ceibal
Not in scale
Generic fractures
Shear fractures
Extensional fractures
Mineralized fractures
Stylolites

kinematic model of progressive positive inversion based on data at various scales, that explains the formation of the regional anticline, the later flower-like structure and the normal faults that dissect it.

We consider that the pre-orogenic normal faults have exerted a strong control on the nucleation and localization of the subsequent thrust ramp development (e.g. Hayward and Graham, 1989). Accordingly, the basement-involved normal fault responsible of the uplift of the anticline, may be transpressionally reactivated as an oblique thrust ramp during the thrust system emplacement since it had a trend oblique with respect to the compression direction (i.e. oblique or transpressional inversion; Butler, 1982; Crane, 1987; McClay, 1989; Lacombe and Mouthereau, 2002). Therefore, a push-up geometry formed during the positive inversion produced the two minor anticlines: *Termas* and *Balboa*.

Many examples derived from seismic interpretation and analogue modeling have demonstrated that in a positive inversion, push-up geometries are related to the transpressional reactivation of pre-existing normal faults (Cooper and Warren, 2010; de Jager, 2003; Deeks and Thomas, 1995; Harding, 1985; Krzywiec et al., 2003; McClay, 1989; Pace and Calamita, 2013; Pace et al., 2012; Vejbaek and Andersen, 1987).

7.2. Implications for geothermal exploration

The results of the qualitative and quantitative structural analysis, carried out on the reservoir and cap rocks, together with the DFN model performed on the reservoir of the studied geothermal system, show that tectonic and fracture network affect fluid circulation (Maffucci et al., 2012a).

NNW–SSE and NE–SW fault planes marking the late stage of positive inversion, can be considered the main structures controlling the migration paths of hot fluids from the reservoir to the surface as demonstrated by some associated calcite-filled fractures well exposed in the area of *Ceibal* and of the *Balboa* and *Termas* anticlines. These mineralized fractures are not included in the DFN model since they are considered impermeable at present for self-sealing processes. Nevertheless, the results of the fracture modeling show that generic fractures with the same orientation, related to the same deformative stage, are characterized by the highest values of permeability (Table 3).

In particular, in the area of the *Balboa* anticline, the upscaling process confirms that the highest values of the secondary permeability are due to the N–S, NNW–SSE and NNE–SSW striking fractures (sets IB, I and IIA, respectively) characterized by the highest values of aperture and frequency (Tables 2, 3). At the same time, in the area of *Ceibal*, modeling shows that the secondary permeability is mainly due to the ENE–WSW and NNE–SSW striking fractures (set II and IIA). On the contrary, the lowest permeability values are localized on the backlimb of the main anticline, in the *Anta Yaco* area (Fig. 13). It depends mainly on the lowest values of aperture of fractures in this area.

Due to the lack of outcrops of the reservoir rock in the northern nose of *Termas* anticline we do not know how fracture network influences fluid circulation in this area at depth. However, fieldwork observations on the overlying cap rock allow us to assume that it played an important role in the upward water flow at surface as we observed that most N–S striking fractures are filled with calcite mineralization.

As a whole, the DFN model performed in the reservoir volume indicates that fracture network enhances its permeability. The results show that the reservoir secondary permeability is of about 49 mD and that its fractured portion represents the 0.03% of the total volume.

Furthermore, the variation of the permeability values in the different sectors of the analyzed structure suggests that the fault planes, responsible of the flower-like structure geometry of the *Sierra de La Candelaria* anticline, may produce a reservoir compartmentalization and their confinement at depth.

In this framework, we interpret that the fault planes trending NE–SW and NNW–SSE in the areas of *Ceibal* and *Hotel Termas*, respectively, represent paths along which fluids move to the surface, occurring with the alignment of the well known hot springs. Moreover, the two faults that confine the reservoir in the three-dimensional reconstruction (the inverted Cretaceous normal fault that borders the anticline to the east and N–S lineament to the west) may act as barriers for the motion of the fluid at depth. Furthermore, taking into account the meteoric origin of the geothermal fluids of the *Hotel Termas* area (Seggiaro et al., 1997), supported by recent isotopic analysis (Chiodi et al., 2012a,b; Invernizzi et al., 2014; Maffucci et al., 2012b), the E–W trending normal fault, dipping to the north and occurring in the central sector of the anticline, together with the outcrops of the permeable sandstones of *Pirgua* Subgroup, may guarantee the effective infiltration of water at depth (Barcelona et al., 2013; Invernizzi et al., 2014; Pierantoni et al., 2012; Seggiaro et al., 1997).

Coupling these results together with the maximum depth values reached by the reservoir (top deeper than 2 km in the area of the northern sector of the regional anticline), the effectiveness of the cap rock in the different areas of the anticline (Di Paolo et al., 2012), the recently performed hydrogeological model of this structure (Invernizzi et al., 2014), we suggest that most favorable site for the potential future exploitation of the geothermal fluids in the *Rosario de La Frontera* area is located along the northern buried plunge of the *Balboa* anticline. This hypothesis is further supported by the presence of a low resistivity anomaly, recently detected by means of AMT investigation (Barcelona et al., 2013), that indicates the occurrence of fluids preserved at shallow depths in the *Pirgua* Subgroup coarse deposits at the core of the *Balboa* anticline.

8. Conclusion

In this contribution we present the results of the reconstruction of the deformation history of the *Sierra de La Candelaria* anticline on the base of structural analysis performed at various scales with the goal to provide a robust tectonic model of the geothermal system of *Rosario de La Frontera* that was missing in the past literature. The new interpretation takes into account a multi-stage model of positive inversion that explains the formation of the regional anticline, the later flower-like structure and the normal faults that dissect it.

Furthermore, the results of the qualitative and quantitative structural analyses, carried on the reservoir and cap rocks, together with the fracture modeling performed on the reservoir of the studied geothermal system, show that tectonic and fracture network affect fluid circulation at depth and control fluid natural upwelling at surface in correspondence to the *Hotel Termas* and *Ceibal* areas. In this framework, we interpret that the NNW–SSE and NE–SW fault planes, associated to the late stage of positive inversion, represent the main structures controlling the migration paths of hot fluids from the reservoir to the surface.

The results of the DFNs corroborate this interpretation showing that the highest values of secondary permeability are due to the fracture sets related to these fault planes. As a whole, the modeling performed indicates that fracture network enhances the permeability of the reservoir.

In conclusion, this work highlights the key role of fieldwork observations in analyzing fractured reservoirs when geophysical data are not available (well data such as cores, borehole images, wireline logs, 3-D seismic profiles).

The proposed methodology allows assessing the quality of the geothermal reservoir of *Rosario de La Frontera* system, on the base of computation of its secondary permeability. It represents an effective alternative to other approaches that are more informative but rarely available. Furthermore, this approach should be taken into account as input to dynamic models and may be greatly improved with additional geological and geophysical data (seismic data, geomechanics, etc.) in order to compute the hydraulic fracture properties and to turn the 3-D DFN into a 3-D fracture porosity and

permeability model suitable for dynamic reservoir simulation and prediction.

8.1. Software

The geological map was elaborated with Esri ArcGis 10. Move 2013 (Midland Valley Ltd.) was used to produce the 3-D geological model and the DFN model. The geometric analysis of mesostructures was computed through the software DAISY3.0 (http://host.uniroma3.it/progetti/fralab/). Fracture length distributions and fisher models (mean orientations and standard deviation) were elaborated using the software EasyFit and the stereo plot tool integrated in Move, respectively. Adobe Illustrator CS5 was also used to produce all the figures.

Acknowledgments

José Viramonte and Walter Baez are warmly thanked for their hospitality in NOA and generous lectures and discussions on Andes geology, in providing unpublished data and logistic support. We kindly acknowledge Pierpaolo Pierantoni and Pablo Caffe, for their precious help in the field and useful scientific discussions. Carlo Ungarelli for insight discussions on the AMT method, Fluvio Esposito for constantly encouraging the realization of this project.

Fundings: Project C.U.I.A. 2011–12 "Esplorazione e utilizzo di risorse geotermiche di media e bassa entalpia in area sub-andina per lo sviluppo energetico sostenibile delle città delle province di Jujuy e Salta" Responsible C. Invernizzi. Miur-PhD Fondo Giovani 2011–2014 to Scuola Dottorale in Geologia del territorio e delle Risorse, Università degli Studi Roma Tre. ex 60% Roma Tre University, Responsible S. Corrado.

This work was also partly funded by "Ministero degli Esteri, Progetto Grande Rilevanza" nr. 00187 (G. Giordano).

References

Allmendinger, R.W., Ramos, V.A., Jordan, T.E., Palma, M., Isacks, B.L., 1983. Paleogeography and Andean structural geometry, northwest Argentina. Tectonics 2, 1–16.
Allmendinger, R.W., Gubbels, T., 1996. Pure and simple shear plateau uplift: Altiplano–Puna, Argentina and Bolivia. Tectonophysics 259, 1–13.
Antonellini, M., Aydin, A., 1994. Effect of faulting on fluid flow in porous sandstones: petrophysical properties. AAPG Bull. 78, 355–377.
Antonellini, M.A., Aydin, A., Pollard, D.D., 1994. Microstructure of deformation bands in porous sandstones at Arches National Park, Utah. J. Struct. Geol. 16, 941–959.
Aydin, A., 2000. Fractures, faults, and hydrocarbon entrapment, migration, and flow. Mar. Pet. Geol. 17, 797–814.
Aydin, A., Johnson, A.M., 1978. Development of faults as deformation bands in porous sandstones. Pure Appl. Geophys. 116, 931–942.
Aydin, A., Johnson, A.M., 1983. Analysis of faulting in porous sandstones. J. Struct. Geol. 5 (1), 19.
Baldis, B.A.J., Gorroño, A., Ploszkiewicz, J.V., Sarudiansky, R.M., 1976. Geotectónica de la Cordillera Oriental, Sierras Subandinas y comarcas adyacientes. Geol. Prov Buenos Aires, Relatorio Congreso Geológico Argentino 6th 1, pp. 4–22.
Barbier, M., Leprêtre, R., Daniel, J.-M., Gasparrini, M., Callot, J.-P., Hamon, Y., Lacombe, O., Floquet, M., 2012. Impact of fracturing stratigraphy on paleo-hydrodynamics, the Madison Formation case study (Bighorn Basin, Wyoming, USA). Tectonophysics 576–577, 116–132.
Barcelona, H., Favetto, A., Peri, V., Pomposiello, C., Ungarelli, C., 2013. The potential of audiomagnetotellurics in the study of geothermal fields: a case study from the northern segment of the La Candelaria Range, northwestern Argentina. J. Appl. Geophys. 88, 83–93.
Barcelona, H., Peri, G., Tobal, J., Sagripanti, L., Favetto, A., 2014. Tectonic activity revealed by morphostructural analysis: development of the Sierra de la Candelaria range, northwestern Argentina. J. S. Am. Earth Sci. 56, 376–395.
Barr, D., Savory, K.E., Fowler, S.R., Arman, K., McGarrity, J.P., 2007. Pre-development fracture modeling in the Clair field, west of Shetland. In: Lonergan, L., Jolly, R.J., Sanderson, D.J., Rawnsley, K.D. (Eds.), Fractured reservoirs. Geological Society (London) Special Publications 270, pp. 205–225.
Beaudoin, N., Bellahsen, N., Lacombe, O., Emmanuel, L., 2011. Fracture-controlled paleohydrogeology in a basement-cored, fault-related fold: Sheep Mountain Anticline, Wyoming, United States. Geochem. Geophys. Geosyst. 12, Q06011. http://dx.doi.org/10.1029/2010GC003494.
Belayneh, M., Geiger, S., Matthäi, S.K., 2006. Numerical simulation of water injection into layered fractured carbonate reservoir analogs. AAPG Bull. 90, 1473–1493.
Bercheñi, V.A., 2003. Hidrogeologia en la cuitad de Rosario de la Frontera y su relacion con la cuenca del Rio Rosario. (Tésis Profesional). Universidad Nacional de Salta, Facultad de Ciencias Naturales, escuela de Geologia.
Bianucci, H., Acevedo, O., Cerdán, J., 1981. Evolución tectosedimentaria del Grupo Salta en la Subcuenca Lomas de Olmedo (provincias de Salta y Formosa). Actas 8th Congreso Geológico Argentino 3, pp. 159–172.
Bianucci, H., Homovc, J.F., Acevedo, O.M., 1982. Inversión tectónica y plegamientos resultantes en la comarca Puesto Guardian-Dos Puntitas, Dpto. Orán, Provincia de Salta. Congreso Nacional de Hidrocarburos. Inst. Argent. del Pet. y del Gas, Buenos Aires.
Bigi, S., Battaglia, M., Alemanni, A., Lombardia, S., Campana, A., Borisova, E., Loizzo, M., 2013. CO2 flow through a fractured rock volume: insights from field data, 3D fractures representation and fluid flow modeling. Int. J. Greenhouse Gas Control 18, 183–199.
Bisdom, K., Gauthier, B.D.M., Bertotti, G., Hardebol, N.J., 2014. Calibrating discrete fracture-network models with a carbonate three-dimensional outcrop fracture network: implications for naturally fractured reservoir modeling. AAPG Bull. 98, 1351–1376.
Bjørlykke, K., 2010. Subsurface water and fluid flow in sedimentary basins. In: Bjørlykke, K. (Ed.), Petroleum Geoscience. From Sedimentary Environments to Rock Physics. Springer, Berlin, pp. 259–279.
Brogi, A., Lazzarotto, A., Liotta, D., Ranalli, G., 2003. Extensional shear zones as imaged by reflection seismic lines: the Larderello geothermal field (central Italy). Tectonophysics 363, 127–139.
Butler, R.W.H., 1982. The terminology of structures in thrust belts. J. Struct. Geol. 4, 239–245.
Cacas, M.C., Ledoux, E., De Marsily, G., Tillie, B., 1990. Modeling fracture flow with a stochastic discrete fracture network: calibration and validation. Water Resour. Res. 26 (3), 479–489.
Cahill, T., Isacks, B., Whitman, D., Chatelain, J.L., Perez, A., Chiu, J.M., 1992. Seismicity and tectonics in Jujuy Province, northwestern Argentina. Tectonics 11, 944–959.
Carrera, N., Muñoz, J.A., 2008. Thrusting evolution in the southern Cordillera Oriental (northern Argentine Andes): constraints from growth strata. Tectonophysics 459, 107–122.
Carrera, N., Muñoz, J.A., Sábat, F., Mon, R., Roca, E., 2006. The role of inversion tectonics in the structure of the Cordillera Oriental (NW Argentinean Andes). J. Struct. Geol. 28 (11), 1921–1932. http://dx.doi.org/10.1016/j.jsg.2006.07.006.
Chiodi, A., Tassi, F., Baez, W., Maffucci, R., Di Paolo, L., Viramonte, J.G., 2012a. Características geoquímicas y isotópicas de los fluidos hidrotermales del sistema geotérmico de Rosario de la Frontera, Sierra de la Candelaria, Salta, Argentina. Congreso Latinoamericano de Hidrogeología y IV Congreso Colombiano de Hidrogeología. Colombia.
Chiodi, A., Tassi, F., Baez, W., Maffucci, R., Di Paolo, L., Viramonte, J.G., 2012b. Chemical and isotope characteristics of the Rosario de la Frontera geothermal fluids, La Candelaria Range (Salta, Argentina). 86° Convegno SGI, Arcavacata di Rende-Cosenza, Settembre. Rend. Online Soc. Geol. Ital. 21, 800–801.
Comníguez, A.H., Ramos, V.A., 1995. Geometry and seismic expression of the Cretaceous Salt Rift System, northwestern Argentina. In: Tankard, A.J., et al. (Eds.), Petroleum basins of South America: American Association of Petroleum Geologists, Memoir 62, pp. 325–340.
Cooper, M., 1992. The analysis of fracture systems in subsurface thrust structures from the foothills of the Canadian Rockies. In: McClay, K.R. (Ed.), Thrust Tectonics. Chapman and Hall, London, pp. 391–405.
Cooper, M.A., Warren, M.J., 2010. The geometric characteristics, genesis and petroleum significance of inversion structures. In: Law, R.D., Butler, R.W.H., Holdsworth, R.E., Krabbendam, M., Strachan, R.A. (Eds.), Continental tectonics and mountain building: the legacy of peach and Horne. Geological Society, London, Special Publications 335, pp. 827–846.
Crane, R.C., 1987. Geologic interpretation of thrust belts. Alaskan North Slope Geol. 2, 621–630.
Cristallini, E., Cominguez, A.H., Ramos, V.A., 1997. Deep structure of the Metán-Guachipas region: tectonic inversion in Northwestern Argentina. J. S. Am. Earth Sci. 10, 403–421.
de Jager, J., 2003. Inverted basins in the Netherlands, similarities and differences. Geol. Mijnb. 82, 339–349.
Deeks, N.R., Thomas, S.A., 1995. Basin inversion in strike-slip regime, the Tornquist Zone, Southern Baltic Sea. In: Buchanan, J.G., Buchanan, P.G. (Eds.), Basin inversion. Geological Society, London, Special Publications 88, pp. 319–338.
Dershowitz, W.S., Einstein, H.H., 1988. Characterizing rock joint geometry with joint system models. Rock Mech. Rock. Eng. 21, 21–51.
Dershowitz, W.S., Herda, H.H., 1992. Interpretation of fracture spacing and intensity. In: Tillerson, J.R., Wawersik, W.R. (Eds.), Proceedings of the 33rd U.S. Symposium on Rock Mechanics. Rotterdam, Balkema, pp. 757–766.
Di Paolo, L., Aldega, L., Corrado, S., Giordano, G., Invernizzi, C., 2012. Modeling of organic and inorganic paleo-thermal indicators to constrain the evolution of the geothermal system of Rosario de La Frontera (La Candelaria Ridge, NW Argentina): a new tool for geothermal exploration. Rend. Online Soc. Geol. Ital. 21, 807–808.
Evans, M.A., Fischer, M.P., 2012. On the distribution of fluids in folds: a review of controlling factors and processes. J. Struct. Geol. 44, 2–24.
Evans, M.A., Hobbs, G.C., 2003. Fate of 'warm' migrating fluids in the central Appalachians during the Late Paleozoic Alleghanian orogeny. J. Geochem. Explor. 78–79, 327–331. http://dx.doi.org/10.1016/S0375-6742(03)00088-8.
Faulkner, D.R., Jackson, C.A.L., Lunn, R., Schlisch, R., Shipton, Z., Wibberley, C., Withjack, M., 2010. A review of recent developments regarding the structure, mechanics and fluid flow properties of fault zones. J. Struct. Geol. 32, 1557–1575.
Fetter, C.W., 1993. Contaminant Hydrogeology. Macmillan, New York, p. 458.
Fischer, M.P., Camilo Higuera-Díaz, I., Evans, M.A., Perry, E.C., Lefticariu, L., 2009. Fracture-controlled paleohydrology in a map-scale detachment fold: insights from the analysis of fluid inclusions in calcite and quartz veins. J. Struct. Geol. 31, 1490–1510.

Fossen, H., Bale, A., 2007. Deformation bands and their influence on fluid flow. AAPG Bull. 91 (12), 1685–1700.
Fossen, H., Hesthammer, J., 1997. Geometric analysis and scaling relations of deformation bands in porous sandstone. J. Struct. Geol. 19, 1479–1493.
Galliski, M.A., Viramonte, J.G., 1988. The Cretaceous paleorift in northwestern Argentina: a petrologic approach. J. S. Am. Earth Sci. 1 (4), 329–342.
Gebhard, J.A., Giudici, A.R., Oliver Gascón, J., 1974. Geología de la comarca entre el río Juramento y arroyo Las Tortugas, provincias de Salta y Jujuy, República Argentina. Rev. Asoc. Geol. Argent. 29 (3), 359–375.
Giordano, G., Pinton, A., Cianfarra, P., Chiodi, A., Baez, W., Viramonte, J., Norini, G., Groppelli, G., 2013. Structural control on geothermal circulation in the Cerro Tuzgle–Tocomar geothermal volcanic area (Puna plateau, Argentina). J. Volcanol. Geotherm. Res. 249, 77–94.
Giordano, G., De Benedetti, A.A., Bonamico, B., Ramazzotti, P., Mattei, M., 2014. Incorporating surface indicators of reservoir permeability into reservoir volume calculations: application to the Colli Albani caldera and the Central Italy Geothermal Province. Earth Sci. Rev. 128, 75–92.
González, O.E., Viruel, M.E., Mon R., Tchilinguirian. Hoja Geológica 2766 - II Tucumán. Boletín 245. Programa Nacional de Cartas Geológicas, 1:250.000. SEGEMAR
Grant, M.A., Donaldson, I.G., Bixley, P.F., 1982. Geothermal Reservoir Engineering. Academic Press, New York, p. 369.
Grier, M., Salfity, J., Allmendiger, R.W., 1991. Andean reactivation of the Cretaceous Salta rift, northwestern Argentina. J. S. Am. Earth Sci. 4, 351–372.
Guerriero, V., Iannace, A., Mazzoli, S., Parente, M., Vitale, S., Giorgioni, M., 2010. Quantifying uncertainties in multi-scale studies of fractured reservoir analogues: implemented statistical analysis of scan line data in carbonate rocks. J. Struct. Geol. 32, 1271–1278. http://dx.doi.org/10.1016/j.jsg.2009.04.016.
Guerriero, V., Vitale, S., Ciarcia, S., Mazzoli, S., 2011. Improved statistical multi-scale analysis of fractured reservoir analogues. Tectonophysics 504, 14–24. http://dx.doi.org/10.1016/j.tecto.2011.01.003.
Guerriero, V., Mazzoli, S., Iannace, A., Vitale, S., Carravetta, A., Strauss, C., 2013. A permeability model for naturally fractured carbonate reservoirs. Mar. Pet. Geol. 40, 115–134.
Gustavson, T.C., Hovorka, S.D., Dutton, A.R., 1994. Origin of satin spar veins in evaporate basins. J. Sediment. Res. A64, 88–94.
Hancock, P.L., 1985. Brittle microtectonics: principles and practice. J. Struct. Geol. 7, 437–457.
Harding, T.P., 1985. Seismic characteristics and identification of negative flower structures, positive flower structures, and positive structural inversion. AAPG Bull. 69, 582–600.
Hayward, A.B., Graham, R.H., 1989. Some geometrical characteristics of inversion. In: Cooper, M.A., Williams, G.D. (Eds.), Inversion tectonics. Geological Society, London, Special Publications 44, pp. 335–347.
Hennings, P.H., Olson, J.E., Thompson, L.B., 2000. Combining outcrop data and three dimensional structural models to characterize fractured reservoirs: an example from Wyoming. AAPG Bull. 84 (6), 830–849.
Iaffa, D.N., Sàbat, F., Muñoz, J.A., Mon, R., Gutierrez, A.A., 2011. The role of inherited structures in a foreland basin evolution. The Metán Basin in NW Argentina. J. Struct. Geol. 33, 1816–1828.
Iaffa, D.N., Sabat, F., Munoz, J.A., Carrera, N., 2013. Basin fragmentation controlled by tectonic inversion and basement uplift in Sierras Pampeanas and Santa Barbára System, northwest Argentina. Geol. Soc. Lond., Spec. Publ. 377.
Invernizzi, C., Pierantoni, P., Chiodi, A., Maffucci, R., Corrado, S., Baez, W., Tassi, F., Giordano, G., Viramonte, J., 2014. Preliminary assessment of the geothermal potential of Rosario de la Frontera area (Salta, NW Argentina): insight from hydro-geological, hydro-geochemical and structural investigations. J. S. Am. Earth Sci. 54, 20–36.
Jafari, A., Babadagli, T., 2011. Effective fracture network permeability of geothermal reservoirs. Geothermics 40, 25–38.
Jamison, W.R., Stearns, D.W., 1982. Tectonic deformation of Wingate Sandstone, Colorado National Monument. AAPG Bull. 66, 2584–2608.
Jolley, S.J., Fisher, Q.J., Ainsworth, R.B., 2010. Reservoir compartmentalization: an introduction. Geol. Soc. Lond., Spec. Publ. 347, 1–8.
Jordan, T.E., Isacks, B., Allmendiger, R.W., Brewer, J.A., Ramos, V.A., Ando, C.J., 1983. Andean tectonics related to geometry of subducted Nazca plate. Bull. Geol. Soc. Am. 94, 341–361.
Kley, J., Monaldi, C.R., 1998. Tectonic shortening and crustal thickness in the Central Andes: how good is the correlation? Geology 26, 723–726.
Kley, J., Monaldi, C.R., 1999. Estructura de las Sierras Subandinas y del sistema de Santa Barbara. Proceedings of the XIV Congreso Geologico, pp. 415–425.
Kley, J., Monaldi, C.R., 2002. Tectonic inversion in the Santa Barbara System of the central Andean foreland thrust belt, northwestern Argentina. Tectonics 21 (6), 1061.
Kranz, R.L., Frankel, A.D., Engelder, T., Scholz, C.H., 1979. The permeability of whole and jointed Barre granite. Int. J. Rock Mech. Min. Sci. Geomech. Abstr. 16, 225–234.
Kress, P.R., 1995. Tectonic inversion of the Subandean Foreland — a combined geophysical and geological approach. Berl. Geowiss. Abh. 23, 120.
Krzywiec, P., Kramarska, R., Zientara, P., 2003. Strike-slip tectonics within the SW Baltic Sea and its relationship to the Mid-Polish Trough inversion evidence from high-resolution seismic data. Tectonophysics 373, 93–105. http://dx.doi.org/10.1016/S0040-1951(03)00286-5.
Lacombe, O., Mouthereau, F., 2002. Basement-involved shortening and deep detachment tectonics in forelands of orogens: Insights from recent collision belts (Taiwan, Western Alps, Pyrenees). Tectonics 21, 1030. http://dx.doi.org/10.1029/2001TC901018.
Laubach, S.E., Ward, M.E., 2006. Diagenesis in porosity evolution of opening-mode fractures, Middle Triassic to Lower Jurassic La Boca Formation, NE Mexico. Tectonophysics 419, 75–97.
Louis, C., 1969. A study of groundwater flow in jointed rock and its influence on the stability of rock masses. Rock Mech. Res. Rep. 10. Imperial College, London.
Maffucci, R., Bigi, S., Chiodi, A., Corrado, S., Di Paolo, L., Giordano, G., 2012a. Fracture modeling applied to the geothermal system potential reservoir of Rosario de La Frontera (La Candelaria Ridge, NW Argentina). Rend. Online Soc. Geol. Ital. 21, 829–831.
Maffucci, R., Caffe, P., Corrado, S., Invernizzi, C., Giordano, G., Pierantoni, P., Viramonte, J., 2012b. La Candelaria Ridge (NW Argentina) as a natural lab for the exploration of the geothermal system of Rosario de La Frontera: methods and preliminary results. Rend. Online Soc. Geol. Ital. 21, 826–828.
Maffucci, R., Bigi, S., Chiodi, A., Corrado, S., Di Paolo, L., Giordano, G., 2013. Reconstruction of a "Discrete Fracture Network" in the geothermal reservoir of Rosario de La Frontera (La Candelaria Ridge, Salta province, NW Argentina). European Geothermal Congress 2013, Pisa, Italy, 3–7 June.
Mair, K., Main, I.G., Elphick, S.C., 2000. Sequential growth of deformation bands in the laboratory. J. Struct. Geol. 22, 25–42.
Manzocchi, T., Childs, C., Walsh, J.J., 2010. Faults and fault properties in hydrocarbon flow models. Geofluids 10, 94–113.
Marchegiani, L., Van Dijk, J.P., Gillespie, P.A., Tondi, E., Cello, G., 2006. Scaling properties of the dimensional and spatial characteristics of fault and fracture systems in the Majella Mountain, central Italy. Geol. Soc. Lond., Spec. Publ. 261, 113–131.
Marquillas, R., Del Papa, C., Sabino, I.F., 2005. Sedimentary aspects and paleoenvironmental evolution of a rift basin: Salta Group (Cretaceous-Paleogene), northwestern Argentina. Int. J. Earth Sci. 94, 94–113.
Marrett, R.A., Allmendinger, R.W., Alonso, R.N., Drake, R.E., 1994. Late Cenozoic tectonic evolution of the Puna Plateau and adjacent foreland, northwestern Argentine Andes. J. S. Am. Earth Sci. 7, 179–207.
Matthai, S.K., Aydin, A., Pollard, D.D., Roberts, S.G., 1998. Simulation of transient well-test signatures for geologically realistic faults in sandstone reservoirs. Soc. Pet. Eng. J. SPE 38442.
McClay, K.R., 1989. Analogue models of inversion tectonics. In: Cooper, M.A., Williams, G.D. (Eds.), Inversion tectonics. Geological Society, London, Special Publications 44, pp. 41–59.
Mon, R., Gutierréz, A., 2007. Estructura del extremo sur del sistema subandino (Provincias de Salta, Santiago del Estero y Tucumán). Rev. Asoc. Geol. Argent. 62 (1), 62–68.
Moreno Espelta, C., Viramonte, J.G., Arias, J.E., 1975. Geología del área termal de Rosario de la Frontera y sus posibilidades geotérmicas. Actas del II Congreso Ibero-Americano de Geología Económica IV, pp. 543–548.
Nelson, R.A., 1992. An approach to evaluating fractured reservoirs. Society of Petroleum Engineers, Annual Technical Conference & Exhibition, San Antonio, October 198, pp. 2167–2170.
Nelson, R.A., 1998. Modern approaches to exploration in fractured reservoirs. AAPG Bull. 82, 1442–1443.
Norini, G., Baez, W., Becchio, R., Viramonte, J.G., Giordano, G., Arnosio, M., Pinton, A., Groppelli, G., 2013. The Calama–Olacapato–El Toro Fault System in the Puna Plateau, Central Andes: geodynamic implications and stratovolcanoes emplacement. Tectonophysics 608, 1280–1297.
Oda, M., 1985. Permeability tensor for discontinuous rock masses. Geotechnique 35, 483–495.
Odling, N.E., Gillespie, P., Bourgine, B., Castaing, C., Chiles, J.P., Christensen, N.P., Fillion, E., Genter, A., Olsen, C., Thrane, L., Trice, R., Aarseth, E., Walsh, J.J., Watterson, J., 1999. Variations in fracture system geometry and their implications for fluid flow in fractured hydrocarbon reservoirs. Pet. Geosci. 5, 373–384.
Olson, J.E., 2003. Sublinear scaling of fracture aperture versus length: an exception or the rule? J. Geophys. Res. 108 (B9), 2413. http://dx.doi.org/10.1029/2001JB000419.
Pace, P., Calamita, F., 2013. Push-up inversion structures v. fault-bend reactivation anticlines along oblique thrust ramps: examples from the Apennines fold-and-thrust belt (Italy). J. Geol. Soc. Lond. http://dx.doi.org/10.1144/jgs2013-053.
Pace, P., Scisciani, V., Calamita, F., Paltrinieri, W., 2012. Positive flower structures as reactivated normal faults along oblique thrust ramps: examples from the Apulian structures, Central–Southern Apennines. Rend. Online Soc. Geol. Ital. 21, 47–49.
Pahl, P.J., 1981. Estimating the mean length of discontinuity traces. Int. J. Rock Mech. Min. Sci. Geomech. Abstr. 18, 221–228.
Pesce, A., Miranda, F., 2003. Catálogo de manifestaciones termales de la República Argentina. Volumen I - Región NoroesteSEGEMAR, Buenos Aires, Argentina.
Pierantoni, P.P., Invernizzi, C., Giordano, C., Corrado, S., Maffucci, R., Chiodi, A., Tassi, F., Viramonte, J., 2012. The geothermal System of Rosario de la Frontera (Salta, Argentina): preliminary geochemical and hydrogeological results. Rend. Online Soc. Geol. Ital. (ISSN: 2035-8008) 22, 186–189.
Priest, S.D., 1993. Discontinuity analysis of rock engineering. Chapman and Hall, London.
Priest, S.D., 2004. Determination of discontinuity size distributions from scanline data. Rock Mech. Rock. Eng. 37, 347–368. http://dx.doi.org/10.1007/s00603-004-0035-2.
Priest, S.D., Hudson, J.A., 1981. Estimation of discontinuity spacing and trace length using scanline surveys. Int. J. Rock Mech. Min. Sci. Geomech. Abstr. 18, 183–197.
Reynolds, J.H., Galli, C.J., Hernandez, R.M., Idleman, B.D., Kotila, J.M., Hilliard, R.V., Naeser, C.W., 2000. Middle Miocene tectonic development of the Transition Zone, Salta Province, northwest Argentina: magnetic stratigraphy from the Metán Subgroup, Sierra de González. GSA Bull. 112, 1736–1751.
Rolleri, E.O., 1976. Sistema de Santa Bárbara, una nueva provincia geológica Argentina. Actas del VI Congreso Geológico Argentino, Bahia Blanca (Argentina). 1, pp. 239–255.
Rouleau, A., Gale, J.E., 1985. Statistical characterization of the fracture system in the Stripa granite, Sweden. Int. J. Rock Mech. Min. Sci. Geomech. 22, 353–367.
Roure, F., Swennen, R., Schneider, F., Faure, J.L., Ferkand, H., Guilhaumou, N., Osadandz, K., Robion, P., Vandeginste, V., 2005. Incidence and importance of tectonics and natural fluid migration on reservoir evolution in foreland fold and thrust belts. Oil Gas Sci. Technol. 60 (1), 67–106. http://dx.doi.org/10.2516/ogst:2005006.
Roure, F., Andriessen, P., Callot, J.-P., Ferket, H., Gonzalez, E., Guilhaumou, N., Hardebol, N., Lacombe, O., Malandain, J., Mougin, P., Muska, K., Ortuno, S., Sassi, W., Swennen, R.,

Vilasi, N., 2010. The use of paleo-thermobarometers and coupled thermal, fluid flow and pore fluid pressure modelling for hydrocarbon and reservoir prediction in fold-and-thrust belts. In: Goffey, G., Craig, J., Needham, T., Scott, R. (Eds.), Hydrocarbons in contractional belts. Geol. Soc. London Spec. Publ. 348, pp. 87–114.
Salfity, J.A., 1982. Evolución paleogeográfica del Grupo Salta (Cretácico-Eogénico), Argentina. V Congreso Latinoamericano de Geología, Actas 1, pp. 11–26.
Salfity, J.A., Marquillas, R.A., 1994. Tectonic and sedimentary evolution of the Cretaceous-Eocene Salta Group, Argentina. In: Salfity, J.A. (Ed.), Cretaceous tectonics of the Andes. Earth Evolution Sciences, Brunswick, Germany, Friedrich Vieweg and Sohn, pp. 266–315.
Salfity, J.A., Monaldi, C., 2006. Hoja Geológica 2566 – IV. Metán. Boletín 319. Programa Nacional de Cartas Geológicas, 1:250.000. SEGEMAR.
Salfity, J.A., Monaldi, C.R., Marquillas, R.A., Gonzáles, R.E., 1993. La inversión tectónica del Umbral de los Gallos en la cuenca del Grupo Salta durante la Fase Incaica, XII Congreso Geologico Argentino and II Congreso de Exploración de Hidrocarburos. Asociación Geológica Argentina, Mendoza, Argentina.
Schultz, R.A., Soliva, R., Fossen, H., Okubo, C.H., Reeves, D.M., 2008. Dependence of displacement-length scaling relations for fractures and deformation bands on the volumetric changes across them. J. Struct. Geol. 30, 1405–1411.
Seggiaro, R.E., Hongn, F.D., 1999. Influencia tectónica en el volcanismo Cenozoico del noroeste argentino. Acta Geol. Hisp. 34, 227–242.
Seggiaro, R., Aguilera, N., Gallardo, E., Ferreti, J., 1995. Structure and geothermal potential of the Rosario de la Frontera termal área. Salta. Argentina. 2. World Geothermal Congress, Florence. Italy, pp. 764–767.
Seggiaro, R., Aguilera, N., Ferretti, J., Gallardo, E., 1997. Estructura del area geotermica de Rosario de la Frontera, Salta, Argentina. Actas VIII Congreso Geologico Chileno, Antofagasta. 1 (2), pp. 390–394.
Shearman, D.J., Mossop, G., Dunsmore, H., Martin, M., 1972. Origin of gypsum veins by hydraulic fracture. Inst. Min. Metall. Trans. Sect. B. Appl. Earth Sci. 81, 149–155.
Shipton, Z.K., Cowie, P.A., 2001. Damage zone and slip-surface evolution over cm to km scales in high-porosity Navajo sandstone Utah. J. Struct. Geol. 23, 1825–1844.
Sibson, R.H., Scott, J., 1998. Stress/fault controls on the containment and release of overpressured fluids: examples from gold–quartz vein systems in Juneau, Alaska, Victoria, Australia and Otago, New Zealand. Ore Geol. Rev. 13, 293–306.
Snow, D.T., 1965. A parallel plate model of fractured permeable media. (PhD Thesis). Univ. of Calif, Berkeley, USA.
Stearns, D.W., 1968. Certain aspect of fracture in naturally deformed rocks. In: Rieker, R.E. (Ed.), National Science Foundation Advanced Science Seminar in Rock Mechanics, Special report. Air Force Cambridge Research Laboratories, Bedford, MA, pp. 97–118.
Sternlof, K.R., Chapin, J.R., Pollard, D.D., Durlofsky, L.J., 2004. Permeability effects of deformation band arrays in sandstone. AAPG Bull. 88, 1315–1329.
Tavani, S., Storti, F., Salvini, F., Toscano, C., 2008. Stratigraphic versus structural control on the deformation pattern associated with the evolution of the Mt. Catria anticline. J. Struct. Geol. 30 (5), 664–681.
Tavani, S., Granado, P., Girundo, M., Iannace, A., Arbues, P., Muñoz, J.A., Mazzoli, S., 2014. Building a virtual outcrop, extracting geological information from it, and sharing the results in Google Earth via OpenPlot and Photoscan: an example from the Khaviz Anticline (Iran). Comput. Geosci. 63, 44–53. http://dx.doi.org/10.1016/j.cageo.2013.10.013.
Terzaghi, R.D., 1964. Source of error in joint surveys. Geotechnique 15, 287–304.
Tsang, Y.W., Witherspoon, P.A., 1981. Hydromechanical behavior of a deformable rock fracture subject to normal stress. J. Geophys. Res. 86, 9287–9298.
Turner, J.C.M., 1959. Estratigrafía del cordón de Escaya y de la sierra de Rinconada (Jujuy). Rev. Asoc. Geol. Argent. 13, 15–39.
Underhill, J.R., Woodcock, N.H., 1987. Faulting mechanisms in high porosity sandstones: New Red Sandstone, Arran, Scotland. In: Jones, M.E., Preston, R.M.F. (Eds.), Deformation of sediments and sedimentary rocks. Geological Society of London Special Publication 29, pp. 91–105.
Van Dijk, J.P., 1998. Analysis and modeling of fractured reservoirs. SPE Paper 50570, Europec. Eur. Pet. Conf. 1, 31–43.
Vejbæk, O.V., Andersen, C., 1987. Cretaceous-early tertiary inversion tectonism in the Danish central trough. Tectonophysics 137, 221–238. http://dx.doi.org/10.1016/0040-1951(87)90321-0.
Vignaroli, G., Pinton, A., De Benedetti, A.A., Giordano, G., Rossetti, F., Soligo, M., Berardi, G., 2013. Structural compartmentalization of a geothermal system, the Torre Alfina field (central Italy). Tectonophysics 608, 482–498.
Viramonte, J.G., Kay, S.M., Becchio, R., Escayola, M., Novitski, I., 1999. Cretaceous rift related magmatism in central–western South America. J. S. Am. Earth Sci. 12, 109–121.
Watanabe, K., Takahashi, H., 1995. Fractal geometry characterization of geothermal reservoir fracture networks. J. Geophys. Res. 100 (B1), 521–528.
Witherspoon, P.A., Wang, J.S.Y., Iwai, K., Gale, J.E., 1980. Validity of cubic law for fluid flow in a deformable rock fracture. Water Resour. Res. 16, 1016–1024.
Wu, H., Pollard, D.D., 1995. An experimental study of the relationship between joint spacing and layer thickness. J. Struct. Geol. 17, 887–905.
Zeeb, C., Gomez-Rivas, E., Bons, P.D., Blum, P., 2013. Evaluation of sampling methods for fracture network characterization using outcrops. AAPG Bull. 97, 1545–1566.